iScience

CellPress
OPEN ACCESS

Article

LETMD1 regulates mitochondrial protein synthesis and import to guard brown fat mitochondrial integrity and function

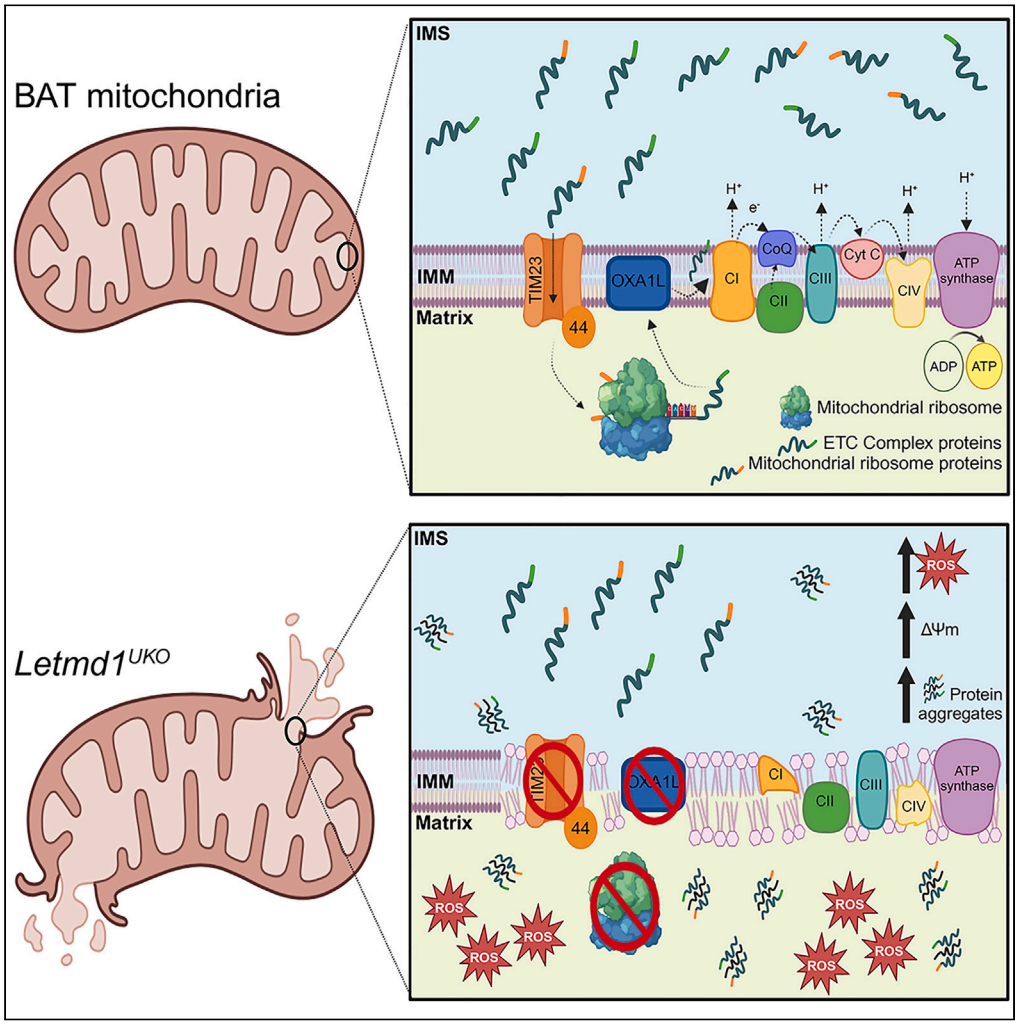

Madigan Snyder, Yi-Kai Liu, Renjie Shang, ..., Pengpeng Bi, W. Andy Tao, Shihuan Kuang

shihuan.kuang@duke.edu

Highlights

LETMD1 localizes to the mitochondrial inner membrane

LETMD1 plays a cell-autonomous role in brown adipocyte integrity and function

LETMD1 is associated with mitochondrial import machinery and ribosomal complexes

LETMD1 regulates mitochondrial protein synthesis, ETC assembly, and respiration

Snyder et al., iScience 27, 110944
October 18, 2024 © 2024 The Author(s). Published by Elsevier Inc.
https://doi.org/10.1016/j.isci.2024.110944

iScience

CellPress
OPEN ACCESS

Article

LETMD1 regulates mitochondrial protein synthesis and import to guard brown fat mitochondrial integrity and function

Madigan Snyder,[1,2] Yi-Kai Liu,[3] Renjie Shang,[4,5] Haowei Xu,[1] Charlie Thrift,[3] Xiyue Chen,[1] Jingjuan Chen,[1,6] Kun Ho Kim,[1] Jiamin Qiu,[1] Pengpeng Bi,[4,5] W. Andy Tao,[3,7] and Shihuan Kuang[1,6,8,*]

SUMMARY

Thermogenic brown adipocytes (BAs) catabolize lipids to generate heat, representing powerful agents against the growing global obesity epidemic. We and others reported recently that LETMD1 is a BA-specific protein essential for mitochondrial structure and function, but the mechanisms of action remain unclear. We performed sequential digestion to demonstrate that LETMD1 is a trans-inner mitochondrial membrane protein. We then generated UCP1Cre-driven BA-specific *Letmd1* knockout (*Letmd1*^{UKO}) mice to show that *Letmd1*^{UKO} leads to protein aggregation, reactive oxidative stress, hyperpolarization, and mitophagy in BAs. We further employed TurboID proximity labeling to identify LETMD1-interacting proteins. Many candidate proteins are associated with mitochondrial ribosomes, protein import machinery, and electron transport chain complexes (ETC-I and ETC-IV). Using quantitative proteomics, we confirmed the elevated aggregations of ETC and mitochondrial ribosomal proteins, impairing mitochondrial protein synthesis in the *Letmd1*^{UKO} BAs. Therefore, LETMD1 may function to maintain mitochondrial proteostasis through regulating import of nuclear-encoded proteins and local protein translation in brown fat mitochondria.

INTRODUCTION

Brown adipose tissue (BAT) is the site of non-shivering thermogenesis within cells and allows for the dissipation of lipid energy as heat.[1] Given the continued rise of obesity within the global population, characterization of BAT is crucial in order to combat energy storage in the form of lipid droplets. Compelling evidence supports that BAT mass is negatively correlated with obesity and body-mass index.[2,3] Previous studies have also shown that adult humans had increased glucose uptake and heat production in BAT when exposed to cold, indicating an additional role for BAT in glucose disposal and beyond (for example as an endocrine organ).[4] Non-shivering thermogenesis takes place within BAT mitochondria, which express uncoupling protein 1 (UCP1), thus permitting the uncoupling of oxidative phosphorylation from ATP synthesis. In addition, BAs may take advantage of the futile creatine cycle, in which creatine and phosphocreatine are continuously interchanged as ATP is consumed, to dissipate energy as heat.[5,6] Regardless, both UCP1 dependent and independent thermogenesis rely largely on mitochondria. Dysfunctional mitochondria are associated with metabolic diseases like obesity.[2] Mitochondrial structure is highly dynamic, and cristae structure remodeling, fusion and fission are critical for thermogenesis and energy expenditure. Therefore, identifying novel regulators of mitochondrial structure and function could lead to new strategies to boost BAT thermogenesis.

We and others have recently reported a key role of LETM1 domain-containing 1 (LETMD1) in brown fat.[7–11] Prior to these emerging studies, LETMD1 was mainly known as a human cervical cancer oncoprotein (HCCR-1) with elevated expression in various tumors, as a negative regulator of p53 function in breast cancer and for its ability to influence expression of inflammatory mediators in macrophages.[12–14] We first reported that global knockout (KO) of *Letmd1* in mice severely compromises the cristae structure and thermogenic function of BAT mitochondria.[7] Our discovery was soon followed by the report of a nuclear function of LETMD1 through its interaction with BRG1 to transcriptionally regulate expression of thermogenic genes.[8] Another group later reported that LETMD1 global KO similarly impairs BAT thermogenesis by impacting mitochondrial Ca^{2+} uptake in BAs.[9] At the same time, quantitative proteomics through the outbred proteome architecture of BAT (OPABAT) project led to the discovery of LETMD1 as a modulator of BAT thermogenesis and adiposity.[10] Most recently, LETMD1 was

[1]Department of Animal Sciences, Purdue University, West Lafayette, IN 47907, USA
[2]Department of Biological Sciences, Purdue University, West Lafayette, IN 47907, USA
[3]Department of Biochemistry, Purdue University, West Lafayette, IN 47907, USA
[4]Center for Molecular Medicine, University of Georgia, Athens, GA 30602, USA
[5]Department of Genetics, University of Georgia, Athens, GA 30602, USA
[6]Department of Orthopaedic Surgery, School of Medicine, Duke University, Durham, NC 27710, USA
[7]Department of Chemistry, Purdue University, West Lafayette, IN 47907, USA
[8]Lead contact
*Correspondence: shihuan.kuang@duke.edu
https://doi.org/10.1016/j.isci.2024.110944

This is an open access article under the CC BY-NC-ND license (http://creativecommons.org/licenses/by-nc-nd/4.0/).

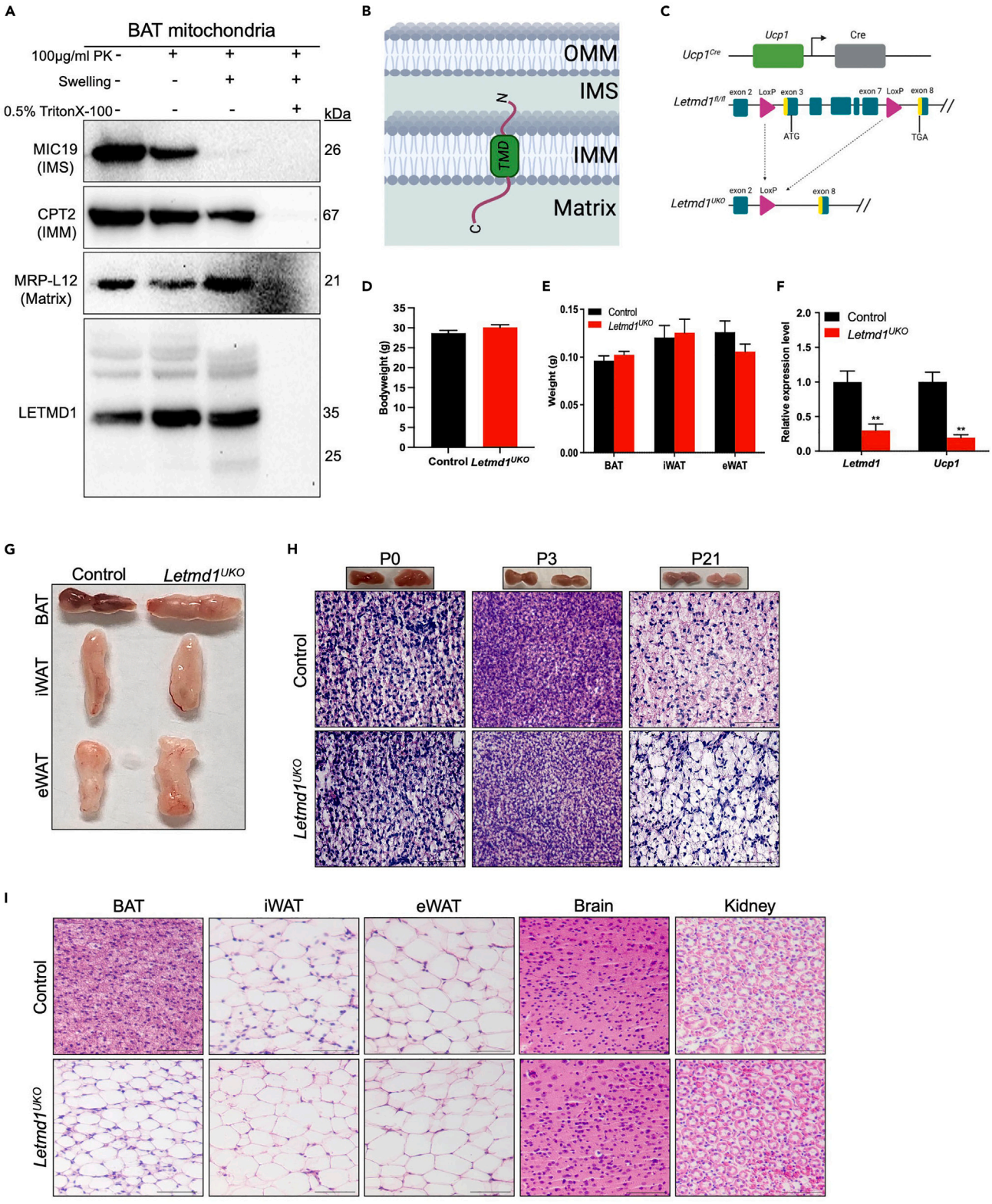
A
BAT mitochondria
100μg/ml PK
Swelling
0.5% TritonX-100
kDa
MIC19 (IMS)
CPT2 (IMM)
MRP-L12 (Matrix)
LETMD1
26
67
21
35
25
B
OMM
IMS
IMM
Matrix
TMD
N
C
C
Ucp1
Cre
Ucp1Cre
Letmd1fl/fl
exon 2
LoxP
exon 3
exon 7
exon 8
ATG
TGA
Letmd1UKO
D
Bodyweight (g)
Control
Letmd1UKO
E
Weight (g)
Control
Letmd1UKO
BAT
iWAT
eWAT
F
Relative expression level
Control
Letmd1UKO
Letmd1
Ucp1
G
Control
Letmd1UKO
BAT
iWAT
eWAT
H
P0
P3
P21
Control
Letmd1UKO
I
BAT
iWAT
eWAT
Brain
Kidney
Control
Letmd1UKO

CellPress
OPEN ACCESS

Figure 1. LETMD1 is a *trans*-IMM protein with a cell autonomous role in BAT

(A) Mitochondrial swelling assay reveals LETMD1 localization on the IMM and matrix-facing portion. The addition of Isotonic buffer and Proteinase K disrupts OMM (Mic19 and CPT2 controls). The addition of Hypotonic buffer and Proteinase K causes swelling of IMM (MRP-L12 control). Hypotonic solution, proteinase K and Triton X-100 burst mitochondria.

(B) Schematic representation of LETMD1 localization on IMM.

(C) Schematic diagram of the Cre-LoxP recombination design used to generate knockout of *Letmd1* (*Letmd1*^{UKO}) in UCP1+ cells.

(D and E) Bodyweight (D) and adipose tissue weights (E) from two-month-old Ctrl and *Letmd1*^{UKO} mice (n = 5).

(F) qPCR analysis of *Letmd1* and *Ucp1* expression in two-month-old CT and *Letmd1*^{UKO} BAT (n = 4).

(G) Representative images of adipose tissues (F) from two-month-old Ctrl and *Letmd1*^{UKO} mice (n = 5).

(H) Representative BAT images and H&E staining of Ctrl and *Letmd1*^{UKO} BAT at different developmental stages, including postnatal day 0 (P0), postnatal day 3 (P3), and postnatal day 21 (P21) (n = 5/stage). Scale bar: 100 μm.

(I) H&E staining of adipose tissues from P60 (two-month-old) Ctrl and *Letmd1*^{UKO} mice. Scale bar: 100 μm.

Data are presented as mean ± SEM. Two-tailed Student's t test, *$p \leq 0.05$, **$p \leq 0.01$. Illustrations were created with Biorender.com.

proposed to localize in the mitochondrial matrix and brown adipocyte-specific *Letmd1* KO mice were shown to phenocopy the global KO mice.[11] Still, a rigorous assessment on the cell-autonomous role of LETMD1 in BAs has yet to be conducted, and the interacting proteins of LETMD1 in the mitochondrion remain unknown.

The UCP1-Cre mouse has been widely used and remains as the best tool available to drive gene KO in BAs, despite the reports that it also targets several non-BA cell types in the brain and kidney.[15,16] In this study, we generated a floxed allele of *Letmd1* to allow BA-specific KO in combination with the UCP1-Cre (*Letmd1*^{UKO}). We found that LETMD1 is required for BAT thermogenesis and mitochondria homeostasis in UCP1+ cells. We further conducted proteomic analyses to investigate the molecular role of LETMD1 in BAT mitochondria and utilized TurboID proximity labeling to identify candidate proteins that interact with LETMD1. Our findings provide a clear connection between LETMD1 and mitochondrial protein import complexes, electron transport chain complexes and ribosomes. These results provide key insights into how LETMD1 functions in mitochondria.

RESULTS

LETMD1 is a *trans*-inner mitochondrial membrane protein

LETMD1 was initially identified as a mitochondrial outer membrane (OMM) protein, but recent publications have proposed it as a mitochondrial inner membrane or matrix protein.[10,11] To clarify the discrepancies, we performed a sequential digestion assay by combining proteinase K with various mitochondrial swelling and permeabilization agents (Figure 1A). We incubated proteinase K (100 μg/mL) with intact mitochondria freshly isolated from BAT to digest only the OMM surface proteins. We then swelled mitochondria in hypotonic buffer to rupture the OMM, allowing proteinase K to additionally digest the intermembrane space (IMS) proteins and inner membrane (IMM) surface proteins but protect the matrix proteins from the digestion. We finally added Triton X-100 to permeabilize the IMM of the swelled mitochondria to allow proteinase K to digest all mitochondrial proteins including the matrix proteins and IMM proteins at the matrix side.

We first set to validate the sequential digestion of several proteins with known localization, using intact mitochondria without any treatments as positive protein loading controls (Figure 1A). The MIC19 protein (encoded by *Chchd3* gene) is known as an IMM protein located on the IMS surface, making it a good control for IMS/IMM protein.[17] Indeed, it was completely digested by proteinase K after swelling (Figure 1A). CPT2 is known to be located to the matrix side of the IMM, making it a control for IMM/Matrix protein. As predicted, CPT2 was digested after swelling and permeabilization (Figure 1A). MRPL12 is a ribosomal protein found in the matrix, and its digestion pattern is also consistent with this known localization (Figure 1A). This observation validates the utility of the sequential digestion assay.

Following this approach, LETMD1 was partially degraded by proteinase K after swelling, as evident from the generation of a smaller band (Figure 1A). This suggests that at least a portion of LETMD1 is exposed to the IMS. LETMD1 was completely degraded by proteinase K after swelling and permeabilization (Figure 1A). This result suggests that at least a portion of LETMD1 is within the matrix. In line with our finding, LETMD1 contains a predicted transmembrane sequence (N#139- LFVGLISIPPFANYLVFLLMYLF-C#161). Based on our digestion results and the predicted transmembrane sequence, we conclude that LETMD1 is a *trans*-IMM protein with a small domain in the IMS side and the majority of the residues facing the matrix (Figure 1B).

A cell-autonomous function of LETMD1 in brown adipocytes

Previous reports on LETMD1 function in BAs are primarily based on global KO models that could indirectly (non-cell-autonomously) impact BAT thermogenesis. To investigate if LETMD1 plays a cell-autonomous role in BAs, we generated a conditional allele (*Letmd1*$^{fl/fl}$) by CRISPR engineering *LoxP* sites into the mouse genome to flank exon 3–exon 7 of *Letmd1* (Figure 1C). We then generated UCP1+ cell-specific knockout mice (*Letmd1*^{UKO}) by crossing the *Letmd1*$^{fl/fl}$ mice with *UCP1-Cre* transgenic mice (Figure 1C). The *Letmd1*^{UKO} mice were born normally and had similar body weight and adipose tissue weights at 2 months of age (Figures 1D and 1E). Upon dissection, whitening of *Letmd1*^{UKO} BAT was apparent, while no obvious differences in iWAT, eWAT, brain, or kidney were observed between Ctrl and *Letmd1*^{UKO} mice (Figure 1G). The normal morphology of brain and kidney suggest that *Letmd1*^{UKO} has no effects on these tissues despite their UCP1-Cre expression.[15,16] Furthermore, the relative level of *Ucp1* was significantly decreased in *Letmd1*^{UKO} BAT, indicating loss of thermogenic function (Figure 1F). H&E staining of paraffin sections also supported age-dependent expansion of unilocular lipid droplets and whitening of the

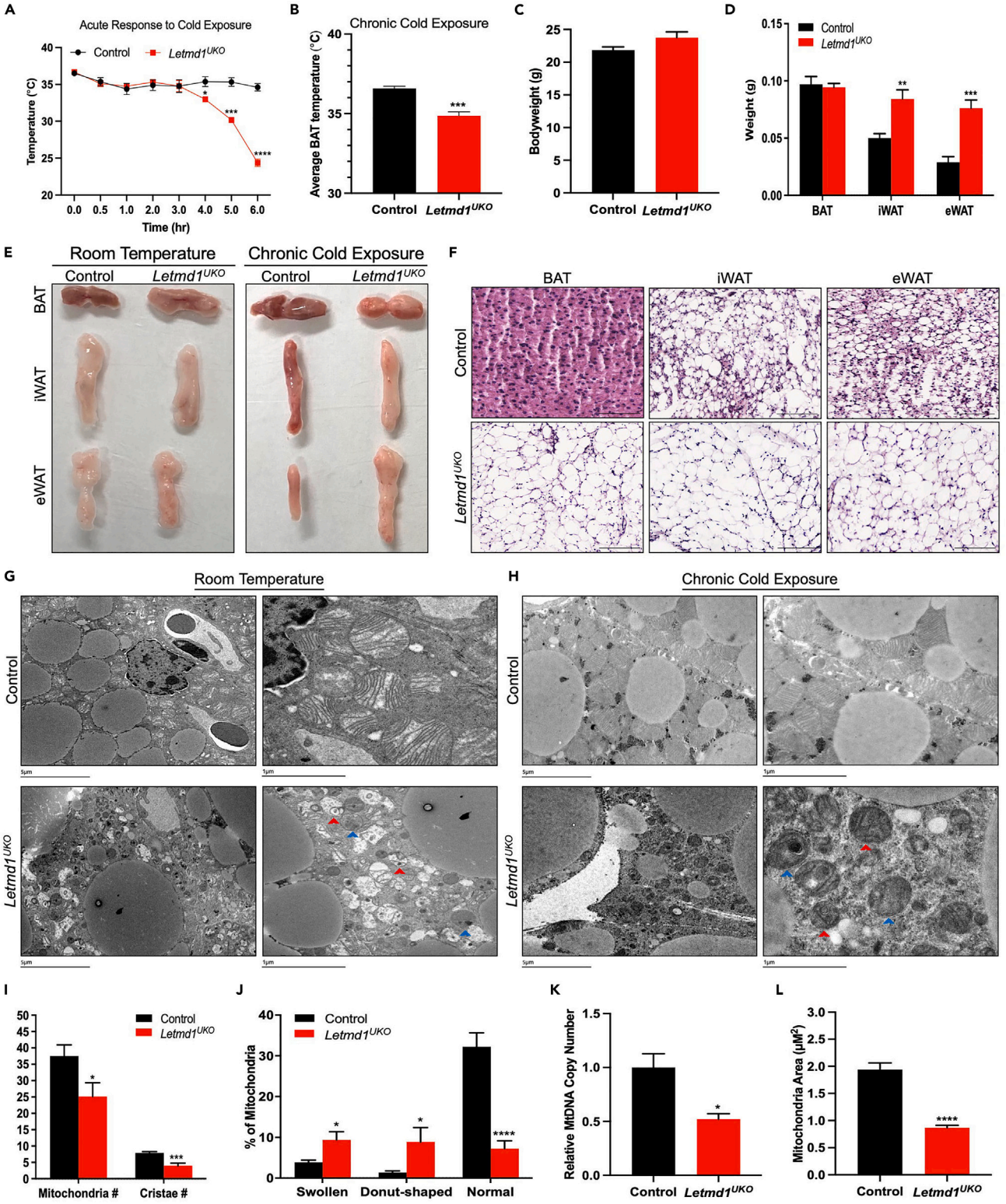

Figure 2. *LETMD1*^{UKO} mice are cold intolerant and exhibit severe mitochondrial defects

(A) Average rectal temperature of two-month-old Ctrl and *Letmd1*^{UKO} mice during acute cold exposure without food (n = 4).

(B) iBAT temperature of Ctrl and *Letmd1*^{UKO} mice upon chronic cold exposure (n = 5).

(C and D) Bodyweight (C) and adipose tissue weights (D) of Ctrl and *Letmd1*^{UKO} mice upon chronic cold exposure (n = 5).

Figure 2. *Continued*

(E) Representative images of adipose tissue from two-month-old Ctrl and *Letmd1*^{UKO} mice at RT and after chronic cold exposure.

(F) H&E staining of adipose tissue from Ctrl and *Letmd1*^{UKO} mice after chronic cold exposure. Scale bar: 100 μm.

(G and H) Representative transmission electron microscopy (TEM) images of Ctrl and *Letmd1*^{UKO} BAT at RT (G) and after chronic cold exposure for 7 days (H). Scale bar for RT and chronic cold TEM lefthand images: 5 μm, righthand images: 1 μm. Red arrows in TEM images indicate swollen mitochondria morphology. Blue arrows indicate donut-shaped mitochondria morphology.

(I and J) Quantification of the mitochondria count per field on TEM image and the number of cristae per mitochondrion (I) and quantification of mitochondria morphology type per field on TEM image (J) in Ctrl and *Letmd1*^{UKO} BAT at room temperature. Eight mitochondria from two pairs of mice were analyzed.

(K) Relative mitochondrial DNA copy number in Ctrl and *Letmd1*^{UKO} BAT at room temperature ($n = 4$).

(L) Quantification of mitochondria area in Ctrl and *Letmd1*^{UKO} BAT. Fifty mitochondria from two pairs of mice were quantified.

Data are presented as mean ± SEM. Two-tailed Student's t test, *$p \leq 0.05$, **$p \leq 0.01$, ***$p \leq 0.001$, ****$p \leq 0.0001$.

Letmd1^{UKO} BAT (Figure 1H). Specifically, the whitening of BAT is not obvious at postnatal day 0 and 3 (P0 and P3). However, BAT whitening is clearly visible in P21 *Letmd1*^{UKO} mice (Figure 1H). At the age of P60, all adipocytes in BAT appeared unilocular, resembling white-adipocyte morphology (Figure 1I). In contrast, no differences in lipid droplet size or accumulation were observed for iWAT and eWAT (Figure 1I). These results demonstrate that LETMD1 plays a cell-autonomous role in BAs, and the loss of LETMD1 results in severe whitening of BAT.

We also performed glucose tolerance test (GTT) and insulin tolerance test (ITT) to understand how BA-specific loss of LETMD1 affects systemic metabolism. No significant differences were observed in glucose disposal or insulin tolerance between Ctrl. and *Letmd1*^{UKO} mice when they were fed on normal chow diet (Figures S2A and S2B). We then performed GTT and ITT on mice after they were fed with a high-fat diet (HFD) for 12 weeks (Figures S2C–S2E). The area under the curve (AUC) for GTT was significantly increased in *Letmd1*^{UKO} mice, suggesting that their ability to clear glucose was significantly hindered (Figure S2D). The area above the curve (AAC) for ITT was mildly decreased in *Letmd1*^{UKO} mice, and the fasting blood glucose level remained slightly elevated in *Letmd1*^{UKO} mice (Figure S2E). Therefore, we conclude that HFD, but not normal chow diet, is sufficient to cause metabolic dysfunction in *Letmd1*^{UKO} mice.

LETMD1^{UKO} mice are cold intolerant and exhibit severe mitochondrial defects

Given that cold-induced non-shivering thermogenesis is an essential component of BAT function, we next subjected two-month-old Ctrl and *Letmd1*^{UKO} mice to acute cold exposure in the absence of food and measured core body temperature over a 6-h period (Figure 2A). While Ctrl mice were able to maintain normal body temperature for the duration of the treatment, the average body temperature of *Letmd1*^{UKO} mice began declining 4 h into treatment, dropping below 30°C by the fifth hour and reaching a drastically low average of 25°C at the 6-h mark. Therefore, the *Letmd1*^{UKO} mice are extremely cold intolerant, as they all fail acute cold exposure.

Mice were then subjected to chronic cold exposure for 7 days with *ad lib* access to food. While Ctrl mice were active and alert (Video S1), *Letmd1*^{UKO} mice appeared lethargic and continuously shivered (Video S2). We immediately measured BAT temperature of each mouse upon removal from the environmental chamber, which revealed that the average BAT temperature of *Letmd1*^{UKO} mice was significantly lower than that of the Ctrl mice (Figure 2B). The average bodyweight of *Letmd1*^{UKO} mice was slightly higher than that of their Ctrl littermates after the 7-day chronic cold treatment (Figure 2C), associated with significantly heavier iWAT and eWAT (Figure 2D), likely due to resistance to cold-induced browning (Figures 2E and 2F) that normally reduces WAT mass. Compared to Ctrl adipose tissue at room temperature (RT), chronic cold exposure also induced noticeable browning of all three adipose tissues in the Ctrl mice but not in the tissues of *Letmd1*^{UKO} mice (Figure 2E). H&E staining revealed the apparent accumulation of multilocular beige adipocytes in Ctrl WAT, but not in WAT of *Letmd1*^{UKO} mice (Figure 2F). The *Letmd1*^{UKO} BAT also maintained unilocular lipid droplets in their cells despite chronic cold exposure (Figure 2F). Furthermore, qPCR analysis of inflammatory markers revealed significantly elevated levels of *Tnfα*, *IL-1β*, and *Adipoq* in *Letmd1*^{UKO} BAT after chronic cold exposure (Figure S3D). Levels of *Tnfα* and *IL-1β* were also significantly higher in *Letmd1*^{UKO} iWAT after chronic cold exposure (Figure S3E), indicating an inflammatory response in both tissues of the *Letmd1*^{UKO}mice. Taken together, *Letmd1*^{UKO} mice exhibit cold intolerance, resistance to cold-induced browning, and elevated inflammation in both BAT and WAT.

We next used transmission electron microscopy (TEM) to examine the mitochondria of *Letmd1*^{UKO} BAT. Examination of BAT from RT and chronic cold-exposed Ctrl and *Letmd1*^{UKO} mice revealed severe abnormalities in *Letmd1*^{UKO} mitochondria structure (Figures 2G and 2H), such as swollen and donut-shaped mitochondria that have been reported to signify mitophagy.[18–21] Many swollen mitochondria exhibited vesicle-like cristae structures that appear puckered (Figures 2G and 2H, red arrows), whereas donut-shaped mitochondria appear either completely void of cristae or contain small, circular cristae structures (Figures 2G and 2H, blue arrows). Quantification of mitochondria and cristae numbers revealed a significant decrease in *Letmd1*^{UKO} BAT (Figure 2I). Additionally, the number of swollen and donut-shaped mitochondria was significantly increased in *Letmd1*^{UKO} BAT, while Ctrl BAT mainly displayed normal mitochondria structures with uniform cristae structure (Figure 2J). Relative mitochondrial DNA copy number was also significantly decreased in *Letmd1*^{UKO} BAT (Figure 2K), consistent with the decreased mitochondria count. Furthermore, the average area of *Letmd1*^{UKO} BAT mitochondria was approximately 50% less than that of Ctrl BAT mitochondria (Figure 2L). Together, these results suggest that LETMD1 is required for normal mitochondria structure and cristae organization in BAs.

Letmd1^{UKO} BAT mitochondria have an altered proteome and exhibit autophagic stress

To understand how UCP1+ cell-specific deletion of *Letmd1* affects mitochondrial structure and function at the molecular level, we isolated mitochondrial protein from three pairs of Ctrl and *Letmd1*^{UKO} BAT and subjected the proteins to mass spectrometry analysis (Figure 3A,

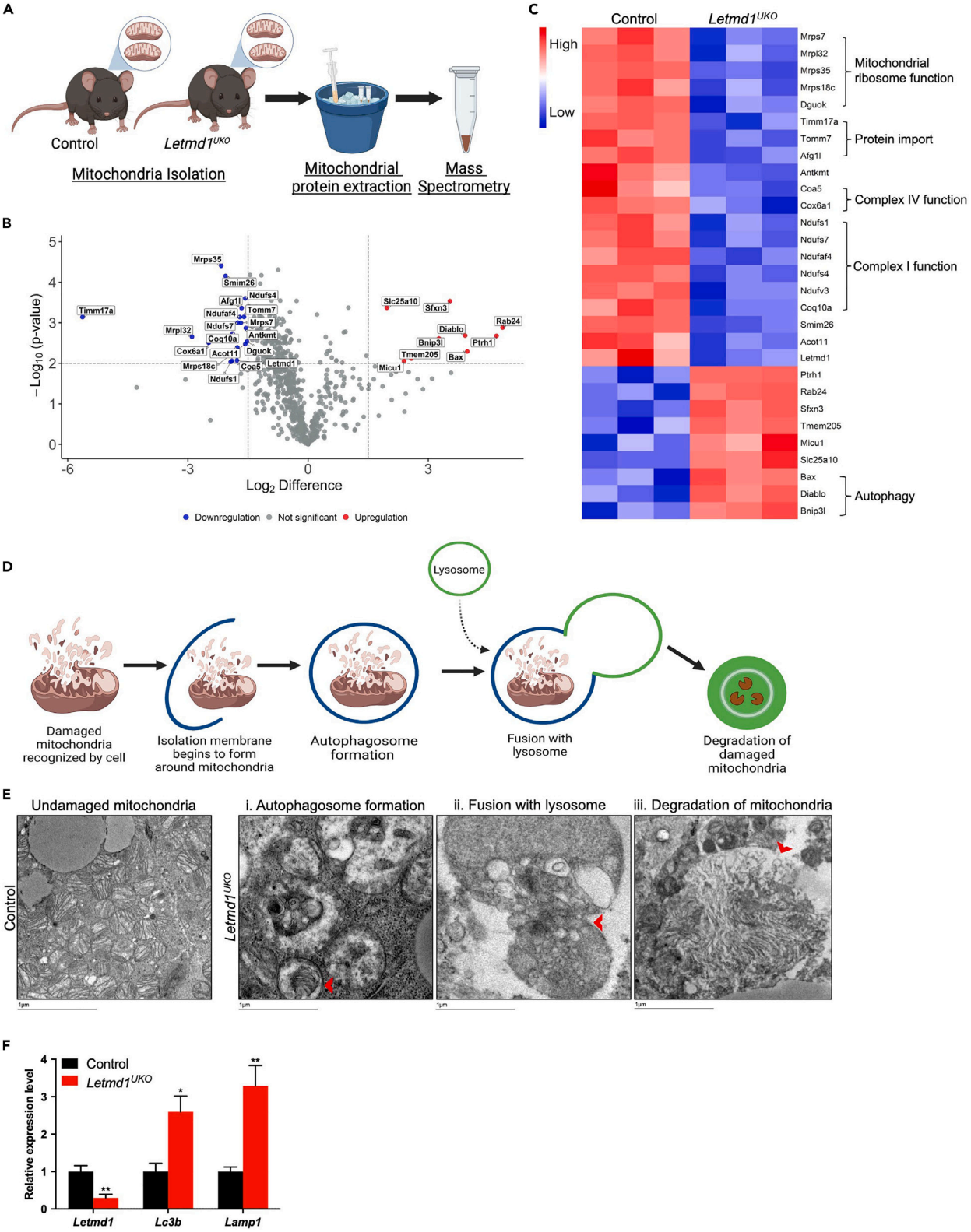
A
Control
Letmd1UKO
Mitochondria Isolation
Mitochondrial protein extraction
Mass Spectrometry
B
−Log10 (p-value)
Log2 Difference
Downregulation
Not significant
Upregulation
C
Control
Letmd1UKO
High
Low
Mitochondrial ribosome function
Protein import
Complex IV function
Complex I function
Autophagy
D
Lysosome
Damaged mitochondria recognized by cell
Isolation membrane begins to form around mitochondria
Autophagosome formation
Fusion with lysosome
Degradation of damaged mitochondria
E
Undamaged mitochondria
i. Autophagosome formation
ii. Fusion with lysosome
iii. Degradation of mitochondria
Control
Letmd1UKO
F
Control
Letmd1UKO
Relative expression level
Letmd1
Lc3b
Lamp1

Figure 3. *Letmd1*^{UKO} BAT mitochondria have an altered proteome and exhibit autophagic stress

(A) Schematic showing mitochondria isolation for mass spectrometry.

(B) Volcano plot of differentially expressed proteins for Ctrl and *Letmd1*^{UKO} BAT mitochondria (n = 3). Each dot represents one protein. Red dots indicate upregulated protein expression in *Letmd1*^{UKO} BAT mitochondria. Blue dots indicate downregulated protein expression in *Letmd1*^{UKO} BAT mitochondria. Log_2 Difference threshold = 1.5. p value threshold = 0.01.

(C) Heatmap of mitochondrial protein expression pattern in Ctrl and *Letmd1*^{UKO} BAT mitochondria (n = 3).

(D) Schematic showing the process of mitophagy, involving the engulfment and degradation of damaged mitochondria.

(E) Representative TEM images of *Letmd1*^{UKO} BAT mitochondria undergoing mitophagy events, including engulfment (i), lysosome fusion (ii) and degradation (iii), in comparison to Ctrl BAT mitochondria. Red arrows indicate the site of mitophagy. Scale bar: 1 μm.

(F) qPCR analysis of autophagy markers *Lc3b* and *Lamp1* in Ctrl and *Letmd1*^{UKO} BAT (n = 4).

Data are presented as mean ± SEM. Two-tailed Student's t test, *$p \leq 0.05$, **$p \leq 0.01$. Illustrations created with Biorender.com.

Proteome Exchange Consortium dataset identifier: PXD051679; PXD054844). Upon filtration and analysis for statistically significant hits, clear protein expression patterns existed between Ctrl and *Letmd1*^{UKO} BAT mitochondria (Figure 3B). Among the 29 differentially expressed proteins, 20 were downregulated and 9 were upregulated in the *Letmd1*^{UKO} BAT mitochondria (Figure 3C). Notably, LETMD1 levels were consistently lower in the *Letmd1*^{UKO} samples (Figure 3C), supporting the validity of the mass spectrometry data. Interestingly, the level of several ETC proteins, specifically complex I (NADH: ubiquinone oxidoreductase) and complex IV (cytochrome *c* oxidase) proteins, were significantly decreased in *Letmd1*^{UKO} BAT mitochondria. Several nuclear-encoded mitochondrial ribosome proteins and the mitochondrial protein import proteins Tomm7, Timm17a, and Afg1l were also significantly decreased in *Letmd1*^{UKO} BAT (Figure 3C). In contrast, autophagy-related proteins were significantly upregulated in *Letmd1*^{UKO} BAT mitochondria (Figure 3C).

Given the elevated levels of autophagy-related proteins (Figure 3C) and the prominent autophagic mitochondria morphology displayed in *Letmd1*^{UKO} BAT (Figures 2G and 2H), we further investigated the distinct mitophagy phases, which can be identified morphologically[18] (Figure 3D). Based on the TEM images of *Letmd1*^{UKO} BAT mitochondria, we were able to identify key mitophagy events taking place within *Letmd1*^{UKO} BAT (Figure 3E). For example, we observed clear visualization of autophagosome formation around mitochondria, the fusion of an autophagosome with a lysosome, and the degradation of mitochondria within a lysosome in *Letmd1*^{UKO} BAT (Figure 3E, red arrows). Consistently, qPCR analysis revealed significantly increased expression of autophagy markers *Lc3b* and *Lamp1* in *Letmd1*^{UKO} BAT (Figure 3F). Taken together, the proteomic, TEM and qPCR analyses provide compelling evidence of elevated mitophagy within *Letmd1*^{UKO} BAs.

Mitophagy is a selective, quality control mechanism that recycles abnormal or stressed mitochondria. To examine if *Letmd1*^{UKO} induces mitochondrial stress, we isolated mature BAs from two-month-old Ctrl and *Letmd1*^{UKO} mice and stained them with CellROX and TMRE, markers of mitochondrial oxidative stress and membrane potential ($\Delta\Psi$m), respectively (Figures 4A and 4B). Quantification revealed significantly increased levels of both ROS and TMRE within *Letmd1*^{UKO} BAs, indicating increased toxicity and hyperpolarization. We also performed Fluo4 staining in mature BAs, and quantification revealed a significantly decreased level of intracellular calcium within *Letmd1*^{UKO} BAs (Figure 4C). Additionally, there was visibly less overlay between Fluo4 and MitoTracker dye in *Letmd1*^{UKO} mature BAs. This correlates with our analysis of hyperpolarization and a more negatively charged *Letmd1*^{UKO} BAT mitochondrial matrix environment. Taken together, the mature BA staining results further support a stressed mitochondrial environment and subsequent mitophagy activity within *Letmd1*^{UKO} BAT.

TurboID reveals a potential role of LETMD1 in mitochondrial protein import

A major obstacle that has hindered our mechanistic understanding of LETMD1 function is the absence of an IP grade LETMD1 antibody for direct pull-down of interacting proteins. Therefore, we utilized TurboID-based proximity labeling as an alternative method to identify potential interaction partners of LETMD1 (Figure 5A). TurboID enlists ATP to convert biotin into biotin-AMP, which can covalently label proteins in the vicinity of 20 nm.[22] Using the Gibson assembly protocol,[23] we constructed a fusion protein linking LETMD1 and TurboID (Figure 5B). Upon transfection and biotin treatment of BAs, we isolated mitochondria for mass spectrometry analysis (Figure 5C, Proteome Exchange Consortium dataset identifier: PXD051679; PXD054844). From the proteomic analysis, we were able to detect a number of enriched proteins that met a Log_2 difference threshold of >1.5 and a p value threshold of <0.01 (Figure 5D). A total of 94 proteins were positively enriched and only 5 were negatively enriched in the Biotin treated group, compared to the negative control group (Figure 5D), supporting the validity of the TurboID labeling.

Consistent with our earlier identification of LETMD1 as a *trans*-IMM protein, all 94 candidate interacting proteins were either IMM or matrix proteins (Figures 5E–5H). Strikingly, many candidate proteins are ETC CI subunit or assembly proteins (Figure 5E). Two CIV assembly factors, COX11 and SURF1, are also IMM proteins (Figure 5E). Another class of candidates that stood out was mitochondrial import machinery proteins (Figure 5F). These include TIMM21 and TIMM44, which are subunits of the translocase of the inner membrane (TIM23) complex, along with HSPD1, HSPE1, and OXA1L. The OXA1L and the TIM23 complexes are known to play a crucial role in mitochondrial protein import and translocation on the inner membrane, including proper insertion of ETC complex proteins.[24–26] An abundance of mitochondrial ribosome proteins was also identified among the candidate proteins (Figure 5G). All ribosomal proteins are involved in synthesis of mitochondrial encoded proteins. Interestingly, all these ribosomal proteins are nuclear-encoded and must be imported into the mitochondrial matrix. This finding correlates with our isolated mitochondria mass spectrometry dataset, in which we detected decreased expression of several mitochondrial ribosome proteins (Figures 3B and 3C). The rest of the candidate proteins have loosely connected functions such as enzymes and membrane transporters (Figure 5H).

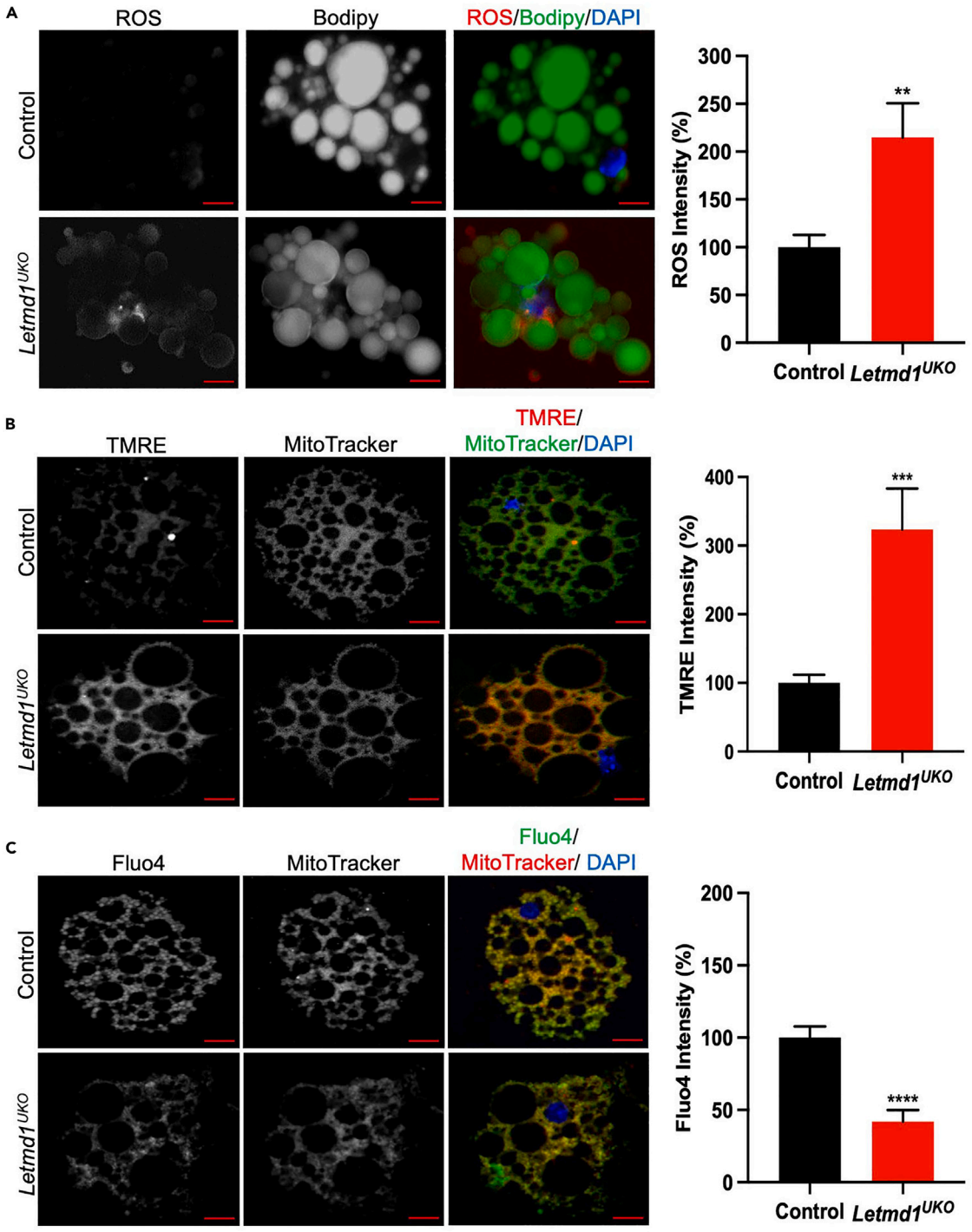

Figure 4. *Letmd1*^{UKO} mature brown adipocytes exhibit mitochondrial stress

(A) Immunofluorescence staining of mature brown adipocytes with ROS. Quantification of ROS intensity reveals a significant increase in *Letmd1*^{UKO} mature brown adipocytes (n = 30 cells quantified/group).

(B) Immunofluorescence staining of mature brown adipocytes with TMRE for mitochondrial membrane potential. Quantification of TMRE intensity reveals a significant increase in *Letmd1*^{UKO} mature brown adipocytes, indicative of hyperpolarization (n = 25 cells quantified/group).

(C) Immunofluorescence staining of mature brown adipocytes with Fluo4 for intracellular calcium. Quantification of Fluo4 intensity reveals a significant decrease in *Letmd1*^{UKO} mature brown adipocytes (n = 32 cells quantified/group). Scale bar: 1 μm.

Data are presented as mean ± SEM. Two-tailed Student's t test, *$p \leq 0.05$, **$p \leq 0.01$, ***$p \leq 0.001$, ****$p \leq 0.0001$.

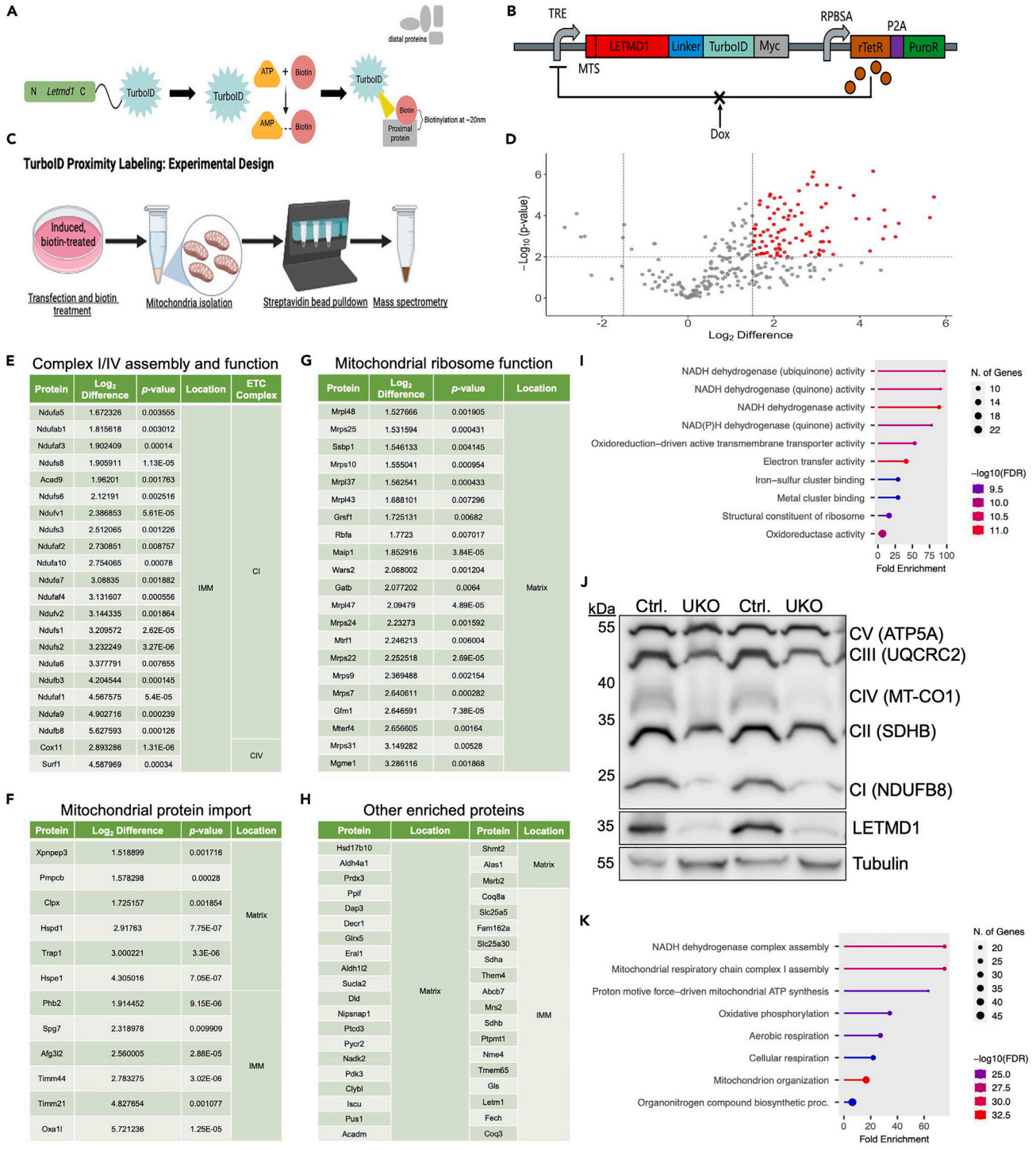

E Complex I/IV assembly and function

Protein	Log2 Difference	p-value	Location	ETC Complex
Ndufa5	1.672326	0.003555	IMM	CI
Ndufab1	1.815618	0.003012		
Ndufaf3	1.902409	0.00014		
Ndufs8	1.905911	1.13E-05		
Acad9	1.96201	0.001763		
Ndufs6	2.12191	0.002516		
Ndufv1	2.386853	5.61E-05		
Ndufs3	2.512065	0.001226		
Ndufaf2	2.730851	0.008757		
Ndufa10	2.754065	0.00078		
Ndufa7	3.08835	0.001882		
Ndufaf4	3.131607	0.000556		
Ndufv2	3.144335	0.001864		
Ndufs1	3.209572	2.62E-05		
Ndufs2	3.232249	3.27E-06		
Ndufa6	3.377791	0.007655		
Ndufb3	4.204544	0.000145		
Ndufaf1	4.567575	5.4E-05		
Ndufa9	4.902716	0.000239		
Ndufb8	5.627593	0.000126		
Cox11	2.893286	1.31E-06		CIV
Surf1	4.587969	0.00034		

F Mitochondrial protein import

Protein	Log2 Difference	p-value	Location
Xpnpep3	1.518899	0.001716	Matrix
Pmpcb	1.578298	0.00028	
Clpx	1.725157	0.001854	
Hspd1	2.91763	7.75E-07	
Trap1	3.000221	3.3E-06	
Hspe1	4.305016	7.05E-07	
Phb2	1.914452	9.15E-06	IMM
Spg7	2.318978	0.009909	
Afg3l2	2.560005	2.88E-05	
Timm44	2.783275	3.02E-06	
Timm21	4.827654	0.001077	
Oxa1l	5.721236	1.25E-05	

G Mitochondrial ribosome function

Protein	Log2 Difference	p-value	Location
Mrpl48	1.527666	0.001905	Matrix
Mrps25	1.531594	0.000431	
Ssbp1	1.546133	0.004145	
Mrps10	1.555041	0.000954	
Mrpl37	1.562541	0.000433	
Mrpl43	1.688101	0.007296	
Grsf1	1.725131	0.00682	
Rbfa	1.7723	0.007017	
Maip1	1.852916	3.84E-05	
Wars2	2.068002	0.001204	
Gatb	2.077202	0.0064	
Mrpl47	2.09479	4.89E-05	
Mrps24	2.23273	0.001592	
Mtrf1	2.246213	0.006004	
Mrps22	2.252518	2.69E-05	
Mrps9	2.369488	0.002154	
Mrps7	2.640611	0.000282	
Gfm1	2.646591	7.38E-05	
Mterf4	2.656605	0.00164	
Mrps31	3.149282	0.00528	
Mgme1	3.286116	0.001868	

H Other enriched proteins

Protein	Location	Protein	Location
Hsd17b10	Matrix	Shmt2	Matrix
Aldh4a1		Alas1	
Prdx3		Msrb2	
Ppif		Coq8a	IMM
Dap3		Slc25a5	
Decr1		Fam162a	
Glrx5		Slc25a30	
Eral1		Sdha	
Aldh1l2		Them4	
Sucla2		Abcb7	
Dld		Mrs2	
Nipsnap1		Sdhb	
Ptcd3		Ptpmt1	
Pycr2		Nme4	
Nadk2		Tmem65	
Pdk3		Gls	
Clybl		Letm1	
Iscu		Fech	
Pus1		Coq3	
Acadm			

Figure 5. TurboID proximity labeling reveals a potential role of LETMD1 in mitochondrial import

(A) Schematic of TurboID proximity labeling. Biotin-AMP can covalently label proteins proximal to LETMD1, up to ~ 20nm. Schematic adapted from Cho et al., 2020.

(B) LETMD1-TurboID fusion protein construct cloned into the pSBtet-Pur plasmid (Addgene #60507), harboring doxycycline-induced expression. The mitochondrial targeting sequence (MTS) of LETMD1 ensures mitochondria localization. The amino acid sequence GGGGSGGG was inserted between LETMD1 and TurboID as a linker. A Myc tag is included for detection in immunoblot and immunofluorescence analysis.

(C) TurboID proximity labeling experimental design for mass spectrometry analysis.

Figure 5. *Continued*

(D) Volcano plot resulting from LETMD1-TurboID proteomic analysis (n = 3). Red dots indicate enriched proteins, using Log2 Difference threshold = 1.5 and p value threshold = 0.01.

(E–G) Tables of enriched proteins of interest, related to ETC complex I and complex IV assembly and function (E), mitochondrial protein import (F) and mitochondrial ribosome assembly and function (G).

(H) List of all other enriched proteins, not of interest, with various functions.

(I) Gene ontology (GO) molecular function analysis of enriched proteins.

(J) Immunoblot analysis showing decreased expression of LETMD1 and electron transport chain complexes CI (NDUFB8), CIV (MT-CO1), and CIII (UQCRC2) in *Letmd1*^{UKO} BAT.

(K) Gene ontology (GO) biological process analysis of enriched proteins. Illustrations created with Biorender.com.

Gene ontology (GO) analysis of the candidate proteins for molecular functions identified all the top four functions as NADH dehydrogenase activity (Figure 5I), which is related to CI. Western blots using a mixture of antibodies detecting CI–CV proteins confirmed that the CI protein (NDUFB8) is the most reduced protein in the *Letmd1*^{UKO} BAT (Figure 5J). The CIV protein MTCO1 and CIII protein UQCRC2 were also noticeably reduced in the *Letmd1*^{UKO} BAT (Figure 5J). Other functions associated with LETMD1 were transmembrane transporter activity and ribosome constituent (Figure 5I), suggesting a potential role of LETMD1 in mitochondrial protein import and synthesis. GO analysis of biological processes confirmed that mitochondrial respiration, especially CI assembly, as the major process associated with LETMD1 (Figure 5K). Mitochondrion organization was another function associated with the LETMD1 labeled proteins (Figure 5K), consistent with its role in mitochondrial cristae structure. In summary, the TurboID proximity labeling reveals a potential connection between LETMD1 and protein import of ribosomal and respiratory chain proteins into mitochondria.

To validate the specific labeling of proteins proximal to LETMD1, we repeated TurboID proximity labeling of BAs with the LETMD1_TurboID fusion protein, or a COX8_TurboID fusion protein as a labeling control. Specifically, the mitochondrial targeting sequence (MTS) for COX8, an IMM protein was fused to TurboID, thereby directing TurboID protein to the IMM where LETMD1 is also located to. After transfection and biotin treatment of the BAs, we isolated mitochondria for mass spectrometry analysis and used a Log_2 difference threshold of >1.5 and a p value threshold of <0.01 for detection of enriched proteins (Figures S4A and S4B). Of the 12 proteins positively enriched in the LETMD1_TurboID biotin treated group (Figure S3B), 8 were also enriched in the initial TurboID labeling experiment (Figures 5E–5H). All 12 proteins are located on the IMM or within the matrix. We detected 6 enriched proteins in BAs labeled with the COX8_TurboID fusion protein, all of which are also located on the IMM or in the matrix (Figure S4A). However, all but one (HSPE1) proteins were different from the LETMD1_TurboID enriched proteins. These results support the specificity of our LETMD1_TurboID labeling.

To validate a potential role for LETMD1 in mitochondrial protein import, we transfected wild type (WT) and global knockout (*Letmd1*^{KO}) BAT SVF cells with a COX8 (MTS)_GFP fusion protein, to monitor its import into the mitochondria. Immunofluorescence staining of BAT SVF cells revealed decreased overlay of GFP with MitoTracker red in *Letmd1*^{KO} BAT SVF cells in comparison to WT SVF cells (Figure S4C). Although GFP intensity does not appear to be significantly decreased in *Letmd1*^{KO} BAT SVF cells, decreased overlay of GFP and MitoTracker red would suggest less mitochondrial protein import resulting from *Letmd1* deletion.

Letmd1^{UKO} BAT exhibits protein aggregates affecting ETC and ribosome protein synthesis

Given the TurboID proximity labeling results, we hypothesized that mitochondrial protein import may be compromised in *Letmd1*^{UKO} BAT. Since the loss of normal mitochondrial protein import can lead to protein misfolding and aggregate formation,[27] this hypothesis predicts that deletion of *Letmd1* may lead to protein aggregates. Misfolded proteins that are unsuccessfully translocated to their proper destination within mitochondria can become insoluble and form protein aggregates, which are reported to cause ROS buildup and mitophagy.[27–30] Indeed, TEM imaging reveals visible protein aggregates inside *Letmd1*^{UKO} BAT mitochondria, whereas Ctrl BAT mitochondria appear mostly free of these aggregates (Figure 6A). The abundance of protein aggregates was further exemplified by quantification, which revealed a 4-fold increase within *Letmd1*^{UKO} BAT mitochondria (Figure 6A).

We then performed biochemical assays to characterize protein solubility in a mild detergent (NP-40). We isolated soluble and insoluble proteins from the cytosolic and mitochondrial fractions of two-month-old Ctrl and *Letmd1*^{UKO} mice (Figure 6B). Protein quantification indicates that both the mitochondrial and cytosolic fractions of the *Letmd1*^{UKO} BAT had significantly higher levels of insoluble proteins when compared to that of the Ctrl BAT (Figures 6C and 6D). Consistent with the elevated aggregates in *Letmd1*^{UKO} mitochondria (Figure 6A), there was a significantly decreased level of soluble proteins in the mitochondria of *Letmd1*^{UKO} mice compared to the Ctrl group (Figure 6D). The increased protein aggregation in *Letmd1*^{UKO} BAT is also consistent with the increased ROS level, hyperpolarization, and mitophagy that we have observed earlier in *Letmd1*^{UKO} mice (Figures 3 and 4).

We further performed mass spectrometry to investigate proteins enriched within the insoluble protein aggregates of Ctrl and *Letmd1*^{UKO} mice (Proteome Exchange Consortium dataset identifier: PXD051679; PXD054844). As protein aggregates were only present within *Letmd1*^{UKO} mitochondria under TEM (Figure 6A), the insoluble protein fractionated from the *Letmd1*^{UKO} cytosol (Figure 6C) may have originated from damaged mitochondria. Therefore, we combined the insoluble protein aggregates isolated from the cytosolic and mitochondrial fractions in the mass spectrometry analysis. A number of enriched proteins related to ETC complexes, mitochondrial protein import, and mitochondrial ribosome function were detected within the insoluble fraction of both Ctrl and *Letmd1*^{UKO} samples (data not shown). We then focused on the proteins whose solubilities were significantly different (protein abundance, $p < 0.01$) in the *Letmd1*^{UKO} and Ctrl samples (Figure 6E; Table S2). We found that the solubility of proteins was predominantly reduced in the *Letmd1*^{UKO} samples, relative to Ctrl

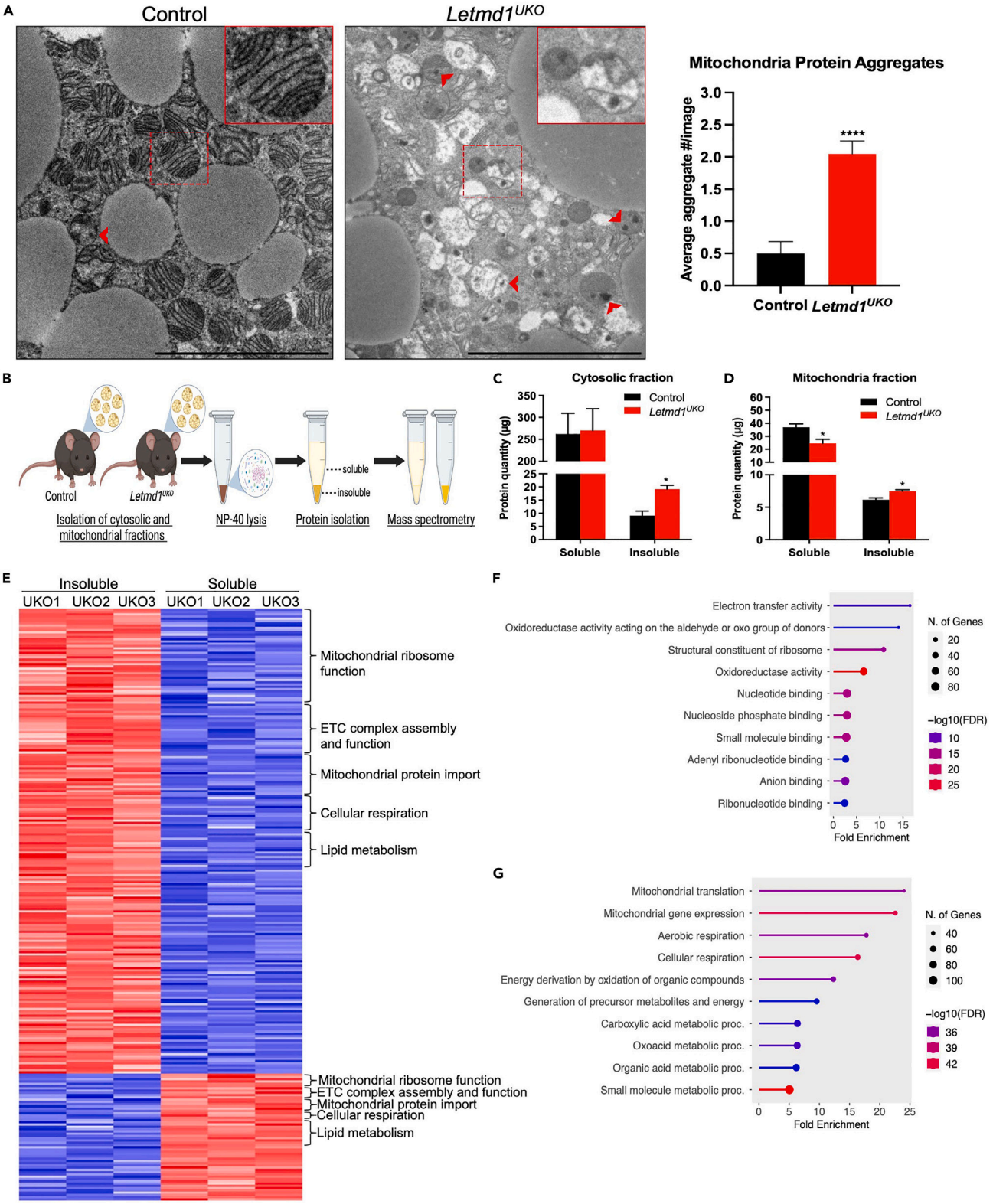
A
Control
Letmd1UKO
Mitochondria Protein Aggregates
Average aggregate #/image
3.0
2.5
2.0
1.5
1.0
0.5
0.0
****
Control
Letmd1UKO
B
Control
Letmd1UKO
soluble
insoluble
Isolation of cytosolic and mitochondrial fractions
NP-40 lysis
Protein isolation
Mass spectrometry
C
Cytosolic fraction
Control
Letmd1UKO
Protein quantity (µg)
350
300
250
200
25
20
15
10
5
0
Soluble
Insoluble
D
Mitochondria fraction
Control
Letmd1UKO
Protein quantity (µg)
60
50
40
30
20
10
5
0
Soluble
Insoluble
E
Insoluble
Soluble
UKO1 UKO2 UKO3 UKO1 UKO2 UKO3
Mitochondrial ribosome function
ETC complex assembly and function
Mitochondrial protein import
Cellular respiration
Lipid metabolism
Mitochondrial ribosome function
ETC complex assembly and function
Mitochondrial protein import
Cellular respiration
Lipid metabolism
F
Electron transfer activity
Oxidoreductase activity acting on the aldehyde or oxo group of donors
Structural constituent of ribosome
Oxidoreductase activity
Nucleotide binding
Nucleoside phosphate binding
Small molecule binding
Adenyl ribonucleotide binding
Anion binding
Ribonucleotide binding
0 5 10 15
Fold Enrichment
N. of Genes
20
40
60
80
–log10(FDR)
10
15
20
25
G
Mitochondrial translation
Mitochondrial gene expression
Aerobic respiration
Cellular respiration
Energy derivation by oxidation of organic compounds
Generation of precursor metabolites and energy
Carboxylic acid metabolic proc.
Oxoacid metabolic proc.
Organic acid metabolic proc.
Small molecule metabolic proc.
0 5 10 15 20 25
Fold Enrichment
N. of Genes
40
60
80
100
–log10(FDR)
36
39
42

Figure 6. *Letmd1*^{UKO} BAT exhibits protein aggregates but increased solubilization of complex I proteins

(A) Representative TEM images of aggregate formation within *Letmd1*^{UKO} BAT mitochondria, compared to Ctrl BAT mitochondria. Red arrows indicate aggregates. Quantification reveals significantly increased protein aggregate formation within *Letmd1*^{UKO} BAT mitochondria. Twenty-two mitochondria from two pairs of mice were quantified. Scale bar: 5 μm.

(B) Schematic showing the experimental design for isolation of cytosolic and mitochondrial fractions from Ctrl and *Letmd1*^{UKO} mice. Illustration created with Biorender.com.

(C) Quantification of soluble and insoluble protein quantity from Ctrl and *Letmd1*^{UKO} cytosolic fractions ($n = 3$).

(D) Quantification of soluble and insoluble protein quantity from Ctrl and *Letmd1*^{UKO} mitochondrial fractions ($n = 3$).

(E) Heatmap of *Letmd1*^{UKO} BAT whole-cell soluble and insoluble proteins ($n = 3$) (p value cutoff <0.01).

(F and G) Gene ontology (GO) analysis for molecular function (F) and biological process (G) of proteins that met significance threshold (p value < 0.01) in *Letmd1*^{UKO} aggregates.

Data are presented as mean ± SEM. Two-tailed Student's t test, *$p \leq 0.05$, **$p \leq 0.01$, ***$p \leq 0.001$, ****$p \leq 0.0001$.

samples (Figure 6E). Among the insoluble proteins enriched in the *Letmd1*^{UKO} samples were ribosome, ETC, protein import, cellular respiration and lipid metabolism associated proteins (Figure 6E). Four CI proteins met the p-value cutoff and were exclusively detected within the *Letmd1*^{UKO} aggregates, but not the Ctrl aggregates. One of these proteins was NDUFV2, which was also enriched within our TurboID mass spectrometry dataset (Figure 5E). Another protein was FAD-dependent oxidoreductase domain-containing protein 1 (FOXRED1), which is reported to be a CI-specific molecular chaperone.[31,32] Furthermore, NDUFAF6, a CI assembly factor, was completely absent from Ctrl aggregates and was only detected within *Letmd1*^{UKO} aggregates. Three CIV proteins, including the subunit COX7A1, were also significantly enriched in *Letmd1*^{UKO} aggregates. Our immunoblot analysis demonstrates drastic loss of CI and CIV proteins (Figure 5J), and the presence of CI and CIV proteins within *Letmd1*^{UKO} aggregates, supports severely compromised protein import and assembly on the IMM.

While an abundance of mitochondrial ribosome proteins were detected in both Ctrl and *Letmd1*^{UKO} whole-cell aggregates, 16 of these proteins were significantly enriched in the *Letmd1*^{UKO} aggregates (Figure 6E; Table S1). All 16 of these mitochondrial ribosome proteins are nuclear encoded and must be imported and translocated to the IMM (MPV17L2) or matrix. Strikingly, we also found that 4 proteins associated with the mitochondrial protein import machinery, including TIMM23, were enriched in the *Letmd1*^{UKO} aggregates. Given that TIMM23 is the major channel-forming subunit of the TIM23 complex on the IMM,[33–35] the aggregation of TIMM23 could hinder the import of IMM and matrix proteins, such as the mitochondrial ribosome proteins. Furthermore, gene ontology analysis of the enriched proteins for molecular function (Figure 6F) and biological process (Figure 6G) revealed a correlation between mitochondrial translation, mitochondrial gene expression and electron transfer activity among the proteins found within *Letmd1*^{UKO} aggregates. Together, these data support our hypothesis that the import and translocation of mitochondrial ribosome and respiratory chain proteins is compromised in *Letmd1*^{UKO} BAT mitochondria.

Given the presence of CI and CIV proteins within *Letmd1*^{UKO} aggregates, we investigated the potential association of LETMD1 with the respiratory chain complexes, by performing 2D blue native PAGE (BN-PAGE). In this assay, ATP5A, SDHB, and NDUFB8 proteins were mainly detected at their predicted 700 kDa (CV), 130 kDa (CII), and 1,000 kDa (CI) positions (Figure 7A), validating the approach. UQCRC2 (CIII) and MTCO1 (CIV) bands were also detected in their expected positions at 490 kDa and 200 kDa, respectively, though they were also detected in other positions (Figure 7A). The results revealed that LETMD1 comigrates with multiple complexes, including a weak association with CI and a moderate association with CIV (Figure 7A). Interestingly, the majority of LETMD1 was detected at around 130 KD position, where CII was predicted to locate. These results suggest that LETMD1 may be independently associated with several mitochondrial ETC complexes.

Given the association of LETMD1 with the respiratory chain and the presence of nuclear-encoded mitochondrial ribosome proteins within *Letmd1*^{UKO}aggregates, we hypothesized that mitochondrial protein synthesis is compromised in *Letmd1*^{UKO} mice. We performed western blot to detect the abundance of mitochondrial and nuclear-encoded proteins, which revealed significantly decreased expression of the mitochondrial-encoded proteins MT-UQCRC2 (CIII), MT-CO1 (CIV) and MT-CO2 (CIV), and MT-ATP6 (CV) (Figure 7B). Consistent with our immunoblot analysis of representative CI–CV proteins (Figure 5J), expression of the nuclear-encoded proteins SDHB (CII) and NDUFB8 (CI) were significantly lower, while ATP5A (CV) expression remained similar in *Letmd1*^{UKO} and Ctrl BAT. These observations indicate that synthesis of mitochondrial-encoded proteins is disrupted upon *Letmd1* deletion. In addition, several proteins synthesized in the cytosol are significantly decreased. These results further reinforce the notion that LETMD1 affects mitochondrial ribosome function and selective import of cytosolic proteins into mitochondria.

DISCUSSION

In this study, we have first elucidated the localization of LETMD1 in the IMM. We then demonstrated that knockout of *Letmd1* in UCP1+ cells renders mice intolerant to cold and abolishes cold-induced browning and thermogenesis, establishing a cell-autonomous function of LETMD1 in BAs. Furthermore, lack of browning in chronic cold-treated WAT (Figure 2F) suggests that LETMD1 impairs the function of both brown and beige adipocytes and is required for mitochondrial protein import and ETC respiratory chain complex assembly. We also used quantitative mass spectrometry, Turbo-ID labeling, TEM, and protein solubility assays to demonstrate that LETMD1 mediates protein import into mitochondria (Figure 7C). In the absence of LETMD1, defective protein import leads to aggregation of respiratory complex and ribosomal proteins, affecting the synthesis and translocation of mitochondrial proteins and assembly of ETC complexes (Figure 7C). These

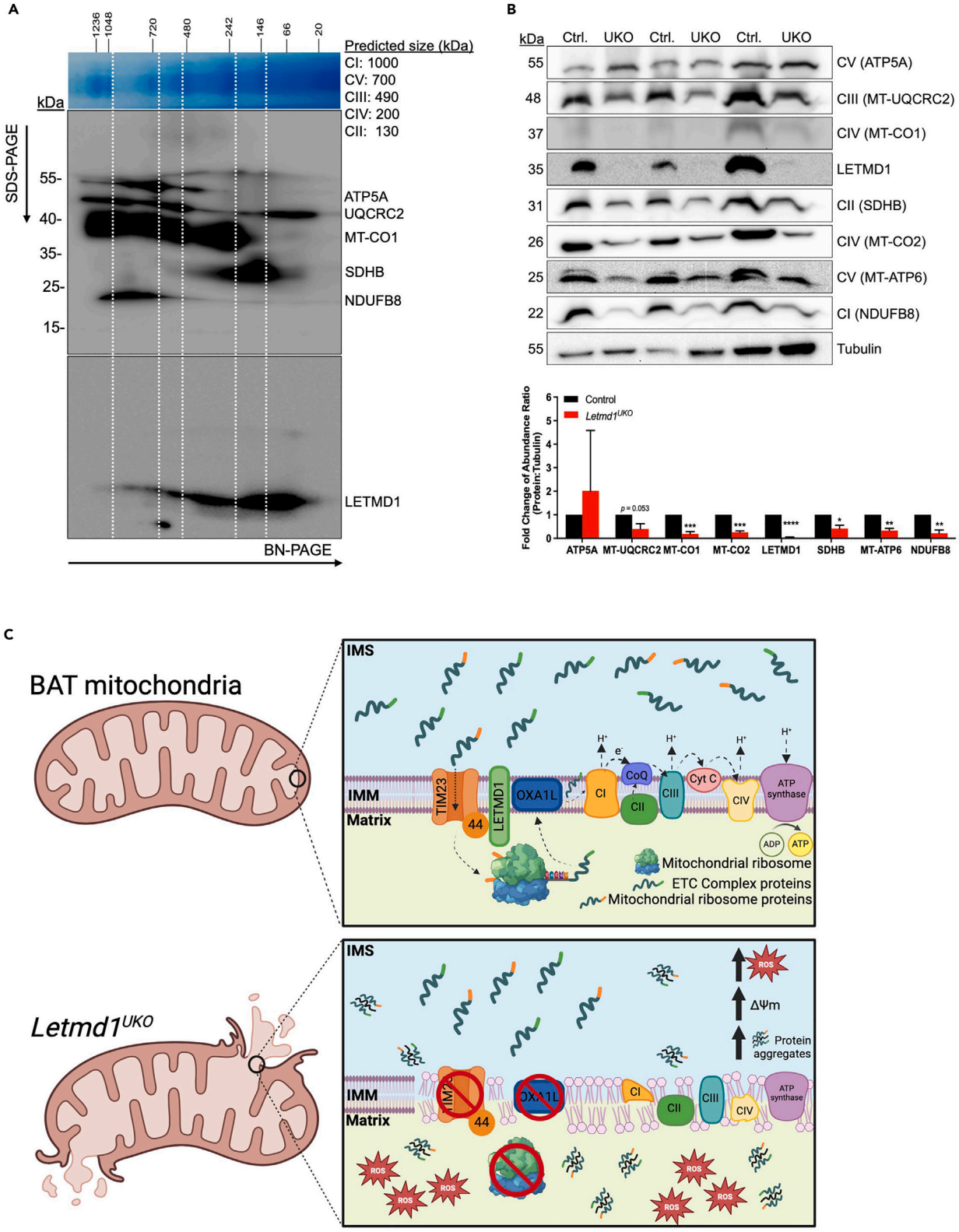
A
1236
1048
720
480
242
146
66
20
Predicted size (kDa)
CI: 1000
CV: 700
CIII: 490
CIV: 200
CII: 130
kDa
SDS-PAGE
55-
40-
35-
25-
15-
ATP5A
UQCRC2
MT-CO1
SDHB
NDUFB8
LETMD1
BN-PAGE
B
kDa
Ctrl.
UKO
Ctrl.
UKO
Ctrl.
UKO
55
48
37
35
31
26
25
22
55
CV (ATP5A)
CIII (MT-UQCRC2)
CIV (MT-CO1)
LETMD1
CII (SDHB)
CIV (MT-CO2)
CV (MT-ATP6)
CI (NDUFB8)
Tubulin
Control
Letmd1UKO
Fold Change of Abundance Ratio (Protein:Tubulin)
p = 0.053
ATP5A
MT-UQCRC2
MT-CO1
MT-CO2
LETMD1
SDHB
MT-ATP6
NDUFB8
C
BAT mitochondria
Letmd1UKO
IMS
IMM
Matrix
TIM23
44
LETMD1
OXA1L
CI
CII
CIII
CIV
CoQ
Cyt C
ATP synthase
ADP
ATP
Mitochondrial ribosome
ETC Complex proteins
Mitochondrial ribosome proteins
ROS
ΔΨm
Protein aggregates

Figure 7. Validation and illustration of LETMD1 association with respiratory chain complexes and mitochondrial protein

(A) Two-dimensional analysis of oxidative phosphorylation complexes and LETMD1. Isolated BAT mitochondria were first separated by blue native electrophoresis (BN-PAGE, horizontal line) followed by denaturing (SDS-PAGE, vertical line).

(B) Immunoblot analysis and quantification of nuclear and mitochondrial-encoded proteins reveals decreased expression of specific respiratory chain proteins.

(C) Summary diagram showing the proposed role of LETMD1 in ribosomal and ETC protein import, mitochondrial protein synthesis and ETC complex assembly on the inner mitochondrial membrane. Illustration created with Biorender.com.

defects further lead to loss of mitochondrial ion homeostasis, elevated reactive oxygen stress, and mitophagy (Figure 7C). These results reveal the physiological function of LETMD1 in the mitochondria.

Previous reports have identified LETMD1 as either IMM or matrix proteins based on different criteria.[10,11] Our conclusion that LETMD1 is a *trans*-IMM protein with N terminus in the IMS and C terminus in the matrix is based on several criteria. The first is the swelling assay digestion pattern; the second is the predicted transmembrane domain; the third is the predicted size after cleaving the N terminus before the transmembrane domain. Additional evidence came from LETMD1-TurboID labeling that only identifies IMM and matrix proteins. While our model is seemingly in disagreement with previous results, it reconciles both reports. In this scenario, LETMD1 can be called an IMM or matrix protein depending on the criteria used. We believe it is most accurate to call LETMD1 a *trans*-IMM protein based on the multiple criteria we and others used and their respective independent observations.

Visualization of autophagic mitochondria morphologies and mitophagy occurring within *Letmd1*^{UKO} BAT highlights the requirement of LETMD1 for normal mitochondria structure and cristae formation. This finding was supported by the increased ROS and $\Delta\Psi$m intensities within *Letmd1*^{UKO} mature BAs. Mitophagy is associated with increased ROS production and loss of normal $\Delta\Psi$m[36–39] and previous studies have reported a positive correlation between ROS and $\Delta\Psi$m.[40–42] Loss of intracellular Ca^{2+} also complements hyperpolarization and a more negatively charged mitochondrial matrix environment within *Letmd1*^{UKO} mature BAs, thus explaining the visible mitophagy and increase in autophagic gene expression we observed in *Letmd1*^{UKO} BAT mitochondria.

Analysis of TurboID mass spectrometry protein hits resulted in the identification of OXA1L, TIMM44, TIMM21, and HSPE1, which could all potentially interact with LETMD1. These findings were intriguing given that several reports implicate the role of protein import translocases in ETC complex assembly.[24,43,44] OXA1L is part of the OXA translocase machinery that mediates the transport of mitochondrial-encoded proteins to the inner membrane.[33,45,46] Several proteins encoded within the mitochondrial ribosome are subunits of ETC complexes, and previous reports have shown that OXA1L is required for the assembly of CI, III, IV, and V.[24,43,47] TIMM21 is part of the TIM23 complex, which is responsible for translocating preproteins to the inner membrane, either by lateral transfer or through transport into the mitochondrial matrix for additional cleavage and subsequent translocation to the inner membrane.[48,49] More specifically, TIMM21 itself is required for the transfer of preproteins from the translocase of the outer membrane (TOM) complex to the TIM23 complex, and this is driven by the inner membrane potential ($\Delta\Psi$). TIMM44 binds preproteins emerging from TIM23 and effectively transports them into the matrix,[33,50,51] which also requires normal $\Delta\Psi$.[52,53] In addition, several reports have suggested that TIMM44 and HSPE1, subunits of the TIM23 complex, interact with the respiratory chain on the inner membrane,[51,54–56] thus requiring normal TIM23 complex function for proper assembly of the ETC. Taken together, both OXA1L and TIM23 translocase machinery are essential for mitochondrial protein import and assembly of ETC complexes, and deletion of *Letmd1* may render both translocases unable to fully insert respiratory chain proteins on the inner mitochondrial membrane.

The 2D blue native PAGE analysis of LETMD1 protein revealed partial comigration with all five complexes in the respiratory chain. However, a portion of the LETMD1 protein does not appear to associate with the respiratory chain at all. Several inner mitochondrial membrane proteins, including LETM1, are reported to associate with the respiratory chain.[57–60] LETM1 is also reported to associate with mitochondrial ribosomes, and LETM1 deletion results in mitochondrial nucleoid aggregation.[61] Furthermore, LETM1 regulates respiratory chain protein synthesis and cristae organization by mediating ion transport on the inner mitochondrial membrane.[57,62–65] Consequently, loss of LETM1 leads to abnormal mitochondria morphology, ion imbalance, and mitophagy.[65–68] Given that LETMD1 contains an LETM1 domain, it is plausible that LETMD1 functions in a similar manner to regulate mitochondrial protein synthesis and ETC complex protein synthesis and assembly on the inner mitochondrial membrane.

In summary, our study confirms the cell autonomous role of LETMD1 in brown adipocyte thermogenic function and mitochondria structure. Deletion of *Letmd1* causes BAT whitening, lipid droplet accumulation, and cold intolerance. *Letmd1*^{UKO} BAT mitochondria exhibit loss of mitochondrial protein import, and more specifically, translocation of complex I and complex IV proteins to the inner membrane for assembly. Protein aggregate formation fuels ROS production, loss of oxidative phosphorylation, and hyperpolarization, resulting in increased mitophagy. These findings exemplify the importance of LETMD1 for mitochondrial homeostasis and BAT thermogenesis.

Limitations of the study

While our conditional knockout of *Letmd1* in UCP1^{+} cells (*Letmd1*^{UKO}) reveals a role for LETMD1 in brown fat mitochondrial function, the underlying mechanism remains to be fully elucidated. We provide evidence that conditional deletion of *Letmd1* ablates brown adipocyte thermogenic function, accompanied by mitochondrial protein aggregation, loss of normal cristae structure and increased mitophagy. Our extensive proteomic analyses revealed LETMD1-interacting proteins that are associated with mitochondrial protein import machinery, mitochondrial ribosomes and electron transport chain complexes I and IV. Proteomic analysis of whole-cell insoluble fractions revealed the presence of mitochondrial ribosome and ETC complex I and IV proteins, further highlighting the requirement of LETMD1 for mitochondrial protein import and synthesis. The validation of LETMD1-interacting proteins identified by TurboID also remains to be completed and represents a key limitation of this study. Although we have performed coimmunoprecipitation (coIP) experiments with several antibodies

recognizing LETMD1-interacting protein candidates, we have not been able to detect LETMD1 bands with any antibody. Given the results of the sequential digestion assay, which revealed that LETMD1 is a matrix-facing, *trans*-IMM protein (Figure 1A), we speculate that the transmembrane configuration of LETMD1 is required for its interaction with candidate proteins. Therefore, the protein isolation procedure required for co-IP may remove LETMD1 from the IMM as it dissolves in the cell lysate, thereby altering LETMD1's 3D structure and limiting its interaction with candidate proteins.

RESOURCE AVAILABILITY

Lead contact

Further information and inquiries regarding resources and reagents should be directed to the lead contact, Shihuan Kuang, Ph.D. (shihuan.kuang@duke.edu).

Materials availability

All unique/stable reagents generated in this study are available form the lead contact with a completed materials transfer agreement.

Data and code availability

- Data reported in this paper will be shared by the lead contact upon request.
- This paper does not report original code. All mass spectrometry raw data files are deposited in the Proteome Exchange Consortium (jPOST). Dataset identifier: PXD051679 and PXD054844.
- Additional information required to reanalyze the data reported in this paper is available from the lead contact upon request.

ACKNOWLEDGMENTS

This work was supported by grants from the National Institutes of Health to S.K. (NIH R01AR078695, R01AR079235, R01DK132819). We thank the Purdue Electron Microscopy facility for TEM sample preparation and imaging guidance, Dr. Junkai Xie and Dr. Chongli Yuan for guidance on Fluo-4 mature adipocyte staining and imaging, Dr. Michael Rudnicki and David Datzkiw for providing guidance on TurboID proximity labeling plasmid construction and optimization, Jun Wu for mouse colony maintenance, and members of the Kuang laboratory for their kind assistance.

AUTHOR CONTRIBUTIONS

S.K. and M.S. conceptualized the project. S.K., M.S., Y.-K.L., R.S., H.X., P.B., and A.T. designed the experiments. M.S., Y.-K.L., R.S., H.X., C.T., X.C., J.C., K.K., and J.Q. performed the experiments. S.K., M.S., and Y.-K.L. analyzed the data. S.K., M.S., and Y.-K.L. wrote the manuscript.

DECLARATION OF INTERESTS

The authors declare no competing interests.

STAR★METHODS

Detailed methods are provided in the online version of this paper and include the following:

- KEY RESOURCES TABLE
- EXPERIMENTAL MODEL AND STUDY PARTICIPANT DETAILS
  - Mice
  - Stromal vascular fraction (SVF) isolation and protein import assay
  - Mature adipocyte isolation
- METHOD DETAILS
  - Hematoxylin-Eosin (H&E) staining
  - Protein extraction and western blot
  - RNA extraction and quantitative PCR (qPCR)
  - Glucose and insulin tolerance tests
  - Cold and thermoneutral exposure experiments
  - Transmission electron microscopy (TEM) imaging
  - DNA extraction and relative mitochondria copy number
  - TurboID proximity labeling
  - Isolation of BAT cytosolic and mitochondrial fractions
  - Isolation of mitochondrial protein aggregates
  - Sample preparation for mass spectrometry-based proteomic analyses
  - LC-MS/MS and raw data analyses
- QUANTIFICATION AND STATISTICAL ANALYSIS

SUPPLEMENTAL INFORMATION

Supplemental information can be found online at https://doi.org/10.1016/j.isci.2024.110944.

Received: May 6, 2024
Revised: July 25, 2024
Accepted: September 10, 2024
Published: September 13, 2024

REFERENCES

1. Bartelt, A., and Heeren, J. (2014). Adipose tissue browning and metabolic health. Nat. Rev. Endocrinol. *10*, 24–36. https://doi.org/10.1038/nrendo.2013.204.
2. Betz, M.J., and Enerbäck, S. (2018). Targeting thermogenesis in brown fat and muscle to treat obesity and metabolic disease. Nat. Rev. Endocrinol. *14*, 77–87. https://doi.org/10.1038/nrendo.2017.132.
3. Matsushita, M., Yoneshiro, T., Aita, S., Kameya, T., Sugie, H., and Saito, M. (2014). Impact of brown adipose tissue on body fatness and glucose metabolism in healthy humans. Int. J. Obes. *38*, 812–817. https://doi.org/10.1038/ijo.2013.206.
4. Virtanen, K.A., Lidell, M.E., Orava, J., Heglind, M., Westergren, R., Niemi, T., Taittonen, M., Laine, J., Savisto, N.J., Enerbäck, S., and Nuutila, P. (2009). Functional brown adipose tissue in healthy adults. N. Engl. J. Med. *360*, 1518–1525. https://doi.org/10.1056/NEJMoa0808949.
5. Rahbani, J.F., Bunk, J., Lagarde, D., Samborska, B., Roesler, A., Xiao, H., Shaw, A., Kaiser, Z., Braun, J.L., Geromella, M.S., et al. (2024). Parallel control of cold-triggered adipocyte thermogenesis by UCP1 and CKB. Cell Metab. *36*, 526–540.e7. https://doi.org/10.1016/j.cmet.2024.01.001.
6. Rahbani, J.F., Roesler, A., Hussain, M.F., Samborska, B., Dykstra, C.B., Tsai, L., Jedrychowski, M.P., Vergnes, L., Reue, K., Spiegelman, B.M., and Kazak, L. (2021). Creatine kinase B controls futile creatine cycling in thermogenic fat. Nature *590*, 480–485. https://doi.org/10.1038/s41586-021-03221-y.
7. Snyder, M.M., Yue, F., Zhang, L., Shang, R., Qiu, J., Chen, J., Kim, K.H., Peng, Y., Oprescu, S.N., Donkin, S.S., et al. (2021). LETMD1 is required for mitochondrial structure and thermogenic function of brown adipocytes. FASEB J. *35*, e21965. https://doi.org/10.1096/fj.202100597R.
8. Choi, K.M., Kim, J.H., Kong, X., Isik, M., Zhang, J., Lim, H.W., and Yoon, J.C. (2021). Defective brown adipose tissue thermogenesis and impaired glucose metabolism in mice lacking Letmd1. Cell Rep. *37*, 110104. https://doi.org/10.1016/j.celrep.2021.110104.
9. Song, R., Du, Y., Li, P., Zhou, L., Zheng, H., Lu, X., Wang, S., Ma, W., Zhang, H., and Li, X. (2022). Deletion of Letmd1 leads to the disruption of mitochondrial function in brown adipose tissue. Biochimie *201*, 100–115. https://doi.org/10.1016/j.biochi.2022.07.002.
10. Xiao, H., Bozi, L.H.M., Sun, Y., Riley, C.L., Philip, V.M., Chen, M., Li, J., Zhang, T., Mills, E.L., Emont, M.P., et al. (2022). Architecture of the outbred brown fat proteome defines regulators of metabolic physiology. Cell *185*, 4654–4673.e28. https://doi.org/10.1016/j.cell.2022.10.003.
11. Park, A., Kim, K.E., Park, I., Lee, S.H., Park, K.Y., Jung, M., Li, X., Sleiman, M.B., Lee, S.J., Kim, D.S., et al. (2023). Mitochondrial matrix protein LETMD1 maintains thermogenic capacity of brown adipose tissue in male mice. Nat. Commun. *14*, 3746. https://doi.org/10.1038/s41467-023-39106-z.
12. Cho, G.W., Shin, S.M., Kim, H.K., Ha, S.A., Kim, S., Yoon, J.H., Hur, S.Y., Kim, T.E., and Kim, J.W. (2007). HCCR-1, a novel oncogene, encodes a mitochondrial outer membrane protein and suppresses the UVC-induced apoptosis. BMC Cell Biol. *8*, 50. https://doi.org/10.1186/1471-2121-8-50.
13. Ko, J., Lee, Y.H., Hwang, S.Y., Lee, Y.S., Shin, S.M., Hwang, J.H., Kim, J., Kim, Y.W., Jang, S.W., Ryoo, Z.Y., et al. (2003). Identification and differential expression of novel human cervical cancer oncogene HCCR-2 in human cancers and its involvement in p53 stabilization. Oncogene *22*, 4679–4689. https://doi.org/10.1038/sj.onc.1206624.
14. Lim, S.G., Suk, K., and Lee, W.H. (2020). LETMD1 Regulates Phagocytosis and Inflammatory Responses to Lipopolysaccharide via Reactive Oxygen Species Generation and NF-κB Activation in Macrophages. J. Immunol. *204*, 1299–1309. https://doi.org/10.4049/jimmunol.1900551.
15. Kim, K., Wann, J., Kim, H.G., So, J., Rosen, E.D., and Roh, H.C. (2024). Uncoupling protein 1-driven Cre (Ucp1-Cre) is expressed in the epithelial cells of mammary glands and various non-adipose tissues. Mol. Metab. *84*, 101948. https://doi.org/10.1016/j.molmet.2024.101948.
16. Claflin, K.E., Flippo, K.H., Sullivan, A.I., Naber, M.C., Zhou, B., Neff, T.J., Jensen-Cody, S.O., and Potthoff, M.J. (2022). Conditional gene targeting using UCP1-Cre mice directly targets the central nervous system beyond thermogenic adipose tissues. Mol. Metab. *55*, 101405. https://doi.org/10.1016/j.molmet.2021.101405.
17. Darshi, M., Mendiola, V.L., Mackey, M.R., Murphy, A.N., Koller, A., Perkins, G.A., Ellisman, M.H., and Taylor, S.S. (2011). ChChd3, an inner mitochondrial membrane protein, is essential for maintaining crista integrity and mitochondrial function. J. Biol. Chem. *286*, 2918–2932. https://doi.org/10.1074/jbc.M110.171975.
18. Chakraborty, J., Caicci, F., Roy, M., and Ziviani, E. (2020). Investigating mitochondrial autophagy by routine transmission electron microscopy: Seeing is believing? Pharmacol. Res. *160*, 105097. https://doi.org/10.1016/j.phrs.2020.105097.
19. Lu, Y., Fujioka, H., Joshi, D., Li, Q., Sangwung, P., Hsieh, P., Zhu, J., Torio, J., Sweet, D., Wang, L., et al. (2018). Mitophagy is required for brown adipose tissue mitochondrial homeostasis during cold challenge. Sci. Rep. *8*, 8251. https://doi.org/10.1038/s41598-018-26394-5.
20. Ahmad, T., Aggarwal, K., Pattnaik, B., Mukherjee, S., Sethi, T., Tiwari, B.K., Kumar, M., Micheal, A., Mabalirajan, U., Ghosh, B., et al. (2013). Computational classification of mitochondrial shapes reflects stress and redox state. Cell Death Dis. *4*, e461. https://doi.org/10.1038/cddis.2012.213.
21. Liu, X., and Hajnóczky, G. (2011). Altered fusion dynamics underlie unique morphological changes in mitochondria during hypoxia-reoxygenation stress. Cell Death Differ. *18*, 1561–1572. https://doi.org/10.1038/cdd.2011.13.
22. Cho, K.F., Branon, T.C., Udeshi, N.D., Myers, S.A., Carr, S.A., and Ting, A.Y. (2020). Proximity labeling in mammalian cells with TurboID and split-TurboID. Nat. Protoc. *15*, 3971–3999. https://doi.org/10.1038/s41596-020-0399-0.
23. Branon, T.C., Bosch, J.A., Sanchez, A.D., Udeshi, N.D., Svinkina, T., Carr, S.A., Feldman, J.L., Perrimon, N., and Ting, A.Y. (2018). Efficient proximity labeling in living cells and organisms with TurboID. Nat. Biotechnol. *36*, 880–887. https://doi.org/10.1038/nbt.4201.
24. Stiburek, L., Fornuskova, D., Wenchich, L., Pejznochova, M., Hansikova, H., and Zeman, J. (2007). Knockdown of human Oxa1l impairs the biogenesis of F1Fo-ATP synthase and NADH:ubiquinone oxidoreductase. J. Mol. Biol. *374*, 506–516. https://doi.org/10.1016/j.jmb.2007.09.044.
25. den Brave, F., Schulte, U., Fakler, B., Pfanner, N., and Becker, T. (2024). Mitochondrial complexome and import network. Trends Cell Biol. *34*, 578–594. https://doi.org/10.1016/j.tcb.2023.10.004.
26. Sánchez-Caballero, L., Guerrero-Castillo, S., and Nijtmans, L. (2016). Unraveling the complexity of mitochondrial complex I assembly: A dynamic process. Biochim. Biophys. Acta *1857*, 980–990. https://doi.org/10.1016/j.bbabio.2016.03.031.
27. Vazquez-Calvo, C., Kohler, V., Höög, J.L., Büttner, S., and Ott, M. (2023). Newly imported proteins in mitochondria are particularly sensitive to aggregation. Acta Physiol. *238*, e13985. https://doi.org/10.1111/apha.13985.
28. Burman, J.L., Pickles, S., Wang, C., Sekine, S., Vargas, J.N.S., Zhang, Z., Youle, A.M., Nezich, C.L., Wu, X., Hammer, J.A., and Youle, R.J. (2017). Mitochondrial fission facilitates the selective mitophagy of protein aggregates. J. Cell Biol. *216*, 3231–3247. https://doi.org/10.1083/jcb.201612106.
29. Lévy, E., El Banna, N., Baïlle, D., Heneman-Masurel, A., Truchet, S., Rezaei, H., Huang, M.E., Béringue, V., Martin, D., and Vernis, L. (2019). Causative Links between Protein Aggregation and Oxidative Stress: A Review. Int. J. Mol. Sci. *20*, 3896. https://doi.org/10.3390/ijms20163896.
30. Samluk, L., Ostapczuk, P., and Dziembowska, M. (2022). Long-term mitochondrial stress induces early steps of Tau aggregation by increasing reactive oxygen species levels and affecting cellular proteostasis. Mol. Biol. Cell *33*, ar67. https://doi.org/10.1091/mbc.E21-11-0553.
31. Fassone, E., Duncan, A.J., Taanman, J.W., Pagnamenta, A.T., Sadowski, M.I., Holand, T., Qasim, W., Rutland, P., Calvo, S.E., Mootha, V.K., et al. (2015). FOXRED1, encoding an FAD-dependent oxidoreductase complex-I-specific molecular chaperone, is mutated in infantile-onset mitochondrial encephalopathy. Hum. Mol. Genet. *24*, 4183. https://doi.org/10.1093/hmg/ddv164.
32. Formosa, L.E., Mimaki, M., Frazier, A.E., McKenzie, M., Stait, T.L., Thorburn, D.R., Stroud, D.A., and Ryan, M.T. (2015). Characterization of mitochondrial FOXRED1 in the assembly of respiratory chain complex I. Hum. Mol. Genet. *24*, 2952–2965. https://doi.org/10.1093/hmg/ddv058.
33. Chacinska, A., Koehler, C.M., Milenkovic, D., Lithgow, T., and Pfanner, N. (2009). Importing mitochondrial proteins: machineries and mechanisms. Cell *138*, 628–644. https://doi.org/10.1016/j.cell.2009.08.005.
34. Alder, N.N., Jensen, R.E., and Johnson, A.E. (2008). Fluorescence mapping of mitochondrial TIM23 complex reveals a water-facing, substrate-interacting helix

surface. Cell *134*, 439–450. https://doi.org/10.1016/j.cell.2008.06.007.

35. Meinecke, M., Wagner, R., Kovermann, P., Guiard, B., Mick, D.U., Hutu, D.P., Voos, W., Truscott, K.N., Chacinska, A., Pfanner, N., and Rehling, P. (2006). Tim50 maintains the permeability barrier of the mitochondrial inner membrane. Science *312*, 1523–1526. https://doi.org/10.1126/science.1127628.
36. Rimessi, A., Bonora, M., Marchi, S., Patergnani, S., Marobbio, C.M.T., Lasorsa, F.M., and Pinton, P. (2013). Perturbed mitochondrial Ca2+ signals as causes or consequences of mitophagy induction. Autophagy *9*, 1677–1686. https://doi.org/10.4161/auto.24795.
37. Cárdenas, C., and Foskett, J.K. (2012). Mitochondrial Ca(2+) signals in autophagy. Cell Calcium *52*, 44–51. https://doi.org/10.1016/j.ceca.2012.03.001.
38. Xiao, B., Kuruvilla, J., and Tan, E.K. (2022). Mitophagy and reactive oxygen species interplay in Parkinson's disease. NPJ Parkinsons Dis. *8*, 135. https://doi.org/10.1038/s41531-022-00402-y.
39. Chen, G., Kroemer, G., and Kepp, O. (2020). Mitophagy: An Emerging Role in Aging and Age-Associated Diseases. Front. Cell Dev. Biol. *8*, 200. https://doi.org/10.3389/fcell.2020.00200.
40. Suski, J., Lebiedzinska, M., Bonora, M., Pinton, P., Duszynski, J., and Wieckowski, M.R. (2018). Relation Between Mitochondrial Membrane Potential and ROS Formation. Methods Mol. Biol. *1782*, 357–381. https://doi.org/10.1007/978-1-4939-7831-1_22.
41. Turrens, J.F. (2003). Mitochondrial formation of reactive oxygen species. J. Physiol. *552*, 335–344. https://doi.org/10.1113/jphysiol.2003.049478.
42. Korshunov, S.S., Skulachev, V.P., and Starkov, A.A. (1997). High protonic potential actuates a mechanism of production of reactive oxygen species in mitochondria. FEBS Lett. *416*, 15–18. https://doi.org/10.1016/s0014-5793(97)01159-9.
43. Thompson, K., Mai, N., Oláhová, M., Scialó, F., Formosa, L.E., Stroud, D.A., Garrett, M., Lax, N.Z., Robertson, F.M., Jou, C., et al. (2018). OXA1L mutations cause mitochondrial encephalopathy and a combined oxidative phosphorylation defect. EMBO Mol. Med. *10*, e9060. https://doi.org/10.15252/emmm.201809060.
44. Cogliati, S., Lorenzi, I., Rigoni, G., Caicci, F., and Soriano, M.E. (2018). Regulation of Mitochondrial Electron Transport Chain Assembly. J. Mol. Biol. *430*, 4849–4873. https://doi.org/10.1016/j.jmb.2018.09.016.
45. Stiller, S.B., Höpker, J., Oeljeklaus, S., Schütze, C., Schrempp, S.G., Vent-Schmidt, J., Horvath, S.E., Frazier, A.E., Gebert, N., van der Laan, M., et al. (2016). Mitochondrial OXA Translocase Plays a Major Role in Biogenesis of Inner-Membrane Proteins. Cell Metab. *23*, 901–908. https://doi.org/10.1016/j.cmet.2016.04.005.
46. Szyrach, G., Ott, M., Bonnefoy, N., Neupert, W., and Herrmann, J.M. (2003). Ribosome binding to the Oxa1 complex facilitates co-translational protein insertion in mitochondria. EMBO J. *22*, 6448–6457. https://doi.org/10.1093/emboj/cdg623.
47. Jia, L., Dienhart, M.K., and Stuart, R.A. (2007). Oxa1 directly interacts with Atp9 and mediates its assembly into the mitochondrial F1Fo-ATP synthase complex. Mol. Biol. Cell *18*, 1897–1908. https://doi.org/10.1091/mbc.e06-10-0925.
48. Popov-Celeketić, D., Mapa, K., Neupert, W., and Mokranjac, D. (2008). Active remodelling of the TIM23 complex during translocation of preproteins into mitochondria. EMBO J. *27*, 1469–1480. https://doi.org/10.1038/emboj.2008.79.
49. Chacinska, A., Lind, M., Frazier, A.E., Dudek, J., Meisinger, C., Geissler, A., Sickmann, A., Meyer, H.E., Truscott, K.N., Guiard, B., et al. (2005). Mitochondrial presequence translocase: switching between TOM tethering and motor recruitment involves Tim21 and Tim17. Cell *120*, 817–829. https://doi.org/10.1016/j.cell.2005.01.011.
50. Krayl, M., Lim, J.H., Martin, F., Guiard, B., and Voos, W. (2007). A cooperative action of the ATP-dependent import motor complex and the inner membrane potential drives mitochondrial preprotein import. Mol. Cell Biol. *27*, 411–425. https://doi.org/10.1128/mcb.01391-06.
51. Slutsky-Leiderman, O., Marom, M., Iosefson, O., Levy, R., Maoz, S., and Azem, A. (2007). The interplay between components of the mitochondrial protein translocation motor studied using purified components. J. Biol. Chem. *282*, 33935–33942. https://doi.org/10.1074/jbc.M704435200.
52. Voos, W., von Ahsen, O., Müller, H., Guiard, B., Rassow, J., and Pfanner, N. (1996). Differential requirement for the mitochondrial Hsp70-Tim44 complex in unfolding and translocation of preproteins. EMBO J. *15*, 2668–2677.
53. Moro, F., Okamoto, K., Donzeau, M., Neupert, W., and Brunner, M. (2002). Mitochondrial protein import: molecular basis of the ATP-dependent interaction of MtHsp70 with Tim44. J. Biol. Chem. *277*, 6874–6880. https://doi.org/10.1074/jbc.M107935200.
54. Wiedemann, N., van der Laan, M., Hutu, D.P., Rehling, P., and Pfanner, N. (2007). Sorting switch of mitochondrial presequence translocase involves coupling of motor module to respiratory chain. J. Cell Biol. *179*, 1115–1122. https://doi.org/10.1083/jcb.200709087.
55. van der Laan, M., Wiedemann, N., Mick, D.U., Guiard, B., Rehling, P., and Pfanner, N. (2006). A role for Tim21 in membrane-potential-dependent preprotein sorting in mitochondria. Curr. Biol. *16*, 2271–2276. https://doi.org/10.1016/j.cub.2006.10.025.
56. Schuler, M.H., Di Bartolomeo, F., Mårtensson, C.U., Daum, G., and Becker, T. (2016). Phosphatidylcholine Affects Inner Membrane Protein Translocases of Mitochondria. J. Biol. Chem. *291*, 18718–18729. https://doi.org/10.1074/jbc.M116.722694.
57. Lupo, D., Vollmer, C., Deckers, M., Mick, D.U., Tews, I., Sinning, I., and Rehling, P. (2011). Mdm38 is a 14-3-3-like receptor and associates with the protein synthesis machinery at the inner mitochondrial membrane. Traffic *12*, 1457–1466. https://doi.org/10.1111/j.1600-0854.2011.01239.x.
58. Murcha, M.W., Kubiszewski-Jakubiak, S., Wang, Y., and Whelan, J. (2014). Evidence for interactions between the mitochondrial import apparatus and respiratory chain complexes via Tim21-like proteins in Arabidopsis. Front. Plant Sci. *5*, 82. https://doi.org/10.3389/fpls.2014.00082.
59. Chen, Y.C., Taylor, E.B., Dephoure, N., Heo, J.M., Tonhato, A., Papandreou, I., Nath, N., Denko, N.C., Gygi, S.P., and Rutter, J. (2012). Identification of a protein mediating respiratory supercomplex stability. Cell Metab. *15*, 348–360. https://doi.org/10.1016/j.cmet.2012.02.006.
60. Mick, D.U., Dennerlein, S., Wiese, H., Reinhold, R., Pacheu-Grau, D., Lorenzi, I., Sasarman, F., Weraarpachai, W., Shoubridge, E.A., Warscheid, B., and Rehling, P. (2012). MITRAC links mitochondrial protein translocation to respiratory-chain assembly and translational regulation. Cell *151*, 1528–1541. https://doi.org/10.1016/j.cell.2012.11.053.
61. Durigon, R., Mitchell, A.L., Jones, A.W., Manole, A., Mennuni, M., Hirst, E.M., Houlden, H., Maragni, G., Lattante, S., Doronzio, P.N., et al. (2018). LETM1 couples mitochondrial DNA metabolism and nutrient preference. EMBO Mol. Med. *10*, e8550. https://doi.org/10.15252/emmm.201708550.
62. Jiang, D., Zhao, L., and Clapham, D.E. (2009). Genome-wide RNAi screen identifies Letm1 as a mitochondrial Ca2+/H+ antiporter. Science *326*, 144–147. https://doi.org/10.1126/science.1175145.
63. Frazier, A.E., Taylor, R.D., Mick, D.U., Warscheid, B., Stoepel, N., Meyer, H.E., Ryan, M.T., Guiard, B., and Rehling, P. (2006). Mdm38 interacts with ribosomes and is a component of the mitochondrial protein export machinery. J. Cell Biol. *172*, 553–564. https://doi.org/10.1083/jcb.200505060.
64. Tamai, S., Iida, H., Yokota, S., Sayano, T., Kiguchiya, S., Ishihara, N., Hayashi, J.I., Mihara, K., and Oka, T. (2008). Characterization of the mitochondrial protein LETM1, which maintains the mitochondrial tubular shapes and interacts with the AAA-ATPase BCS1L. J. Cell Sci. *121*, 2588–2600. https://doi.org/10.1242/jcs.026625.
65. Nakamura, S., Matsui, A., Akabane, S., Tamura, Y., Hatano, A., Miyano, Y., Omote, H., Kajikawa, M., Maenaka, K., Moriyama, Y., et al. (2020). The mitochondrial inner membrane protein LETM1 modulates cristae organization through its LETM domain. Commun. Biol. *3*, 99. https://doi.org/10.1038/s42003-020-0832-5.
66. Piao, L., Li, Y., Kim, S.J., Byun, H.S., Huang, S.M., Hwang, S.K., Yang, K.J., Park, K.A., Won, M., Hong, J., et al. (2009). Association of LETM1 and MRPL36 contributes to the regulation of mitochondrial ATP production and necrotic cell death. Cancer Res. *69*, 3397–3404. https://doi.org/10.1158/0008-5472.Can-08-3235.
67. Nowikovsky, K., Reipert, S., Devenish, R.J., and Schweyen, R.J. (2007). Mdm38 protein depletion causes loss of mitochondrial K+/H+ exchange activity, osmotic swelling and mitophagy. Cell Death Differ. *14*, 1647–1656. https://doi.org/10.1038/sj.cdd.4402167.
68. Dimmer, K.S., Navoni, F., Casarin, A., Trevisson, E., Endele, S., Winterpacht, A., Salviati, L., and Scorrano, L. (2008). LETM1, deleted in Wolf-Hirschhorn syndrome is required for normal mitochondrial morphology and cellular viability. Hum. Mol. Genet. *17*, 201–214. https://doi.org/10.1093/hmg/ddm297.
69. Ohtsuka, M., Sato, M., Miura, H., Takabayashi, S., Matsuyama, M., Koyano, T., Arifin, N., Nakamura, S., Wada, K., and Gurumurthy, C.B. (2018). i-GONAD: a robust method for *in situ* germline genome engineering using CRISPR nucleases.

Genome Biol. *19*, 25. https://doi.org/10.1186/s13059-018-1400-x.

70. Dimauro, I., Pearson, T., Caporossi, D., and Jackson, M.J. (2012). A simple protocol for the subcellular fractionation of skeletal muscle cells and tissue. BMC Res. Notes *5*, 513. https://doi.org/10.1186/1756-0500-5-513.
71. Franco-Iborra, S., Cuadros, T., Parent, A., Romero-Gimenez, J., Vila, M., and Perier, C. (2018). Defective mitochondrial protein import contributes to complex I-induced mitochondrial dysfunction and neurodegeneration in Parkinson's disease. Cell Death Dis. *9*, 1122. https://doi.org/10.1038/s41419-018-1154-0.
72. Rath, S., Sharma, R., Gupta, R., Ast, T., Chan, C., Durham, T.J., Goodman, R.P., Grabarek, Z., Haas, M.E., Hung, W.H.W., et al. (2021). MitoCarta3.0: an updated mitochondrial proteome now with sub-organelle localization and pathway annotations. Nucleic Acids Res. *49*. D1541-d1547. https://doi.org/10.1093/nar/gkaa1011.
73. Ge, S.X., Jung, D., and Yao, R. (2020). ShinyGO: a graphical gene-set enrichment tool for animals and plants. Bioinformatics *36*, 2628–2629. https://doi.org/10.1093/bioinformatics/btz931.
74. Wittig, I., Braun, H.P., and Schägger, H. (2006). Blue native PAGE. Nat. Protoc. *1*, 418–428. https://doi.org/10.1038/nprot.2006.62.

STAR★METHODS

KEY RESOURCES TABLE

REAGENT or RESOURCE	SOURCE	IDENTIFIER
Antibodies		
Rabbit Polyclonal anti-LETMD1/HCCR-1	Abcam	Cat # ab175410
Rabbit Polyclonal anti-Tubulin	Abcam	Cat #: ab6046, RRID: AB_2210370
Mouse Monoclonal anti-CHCHD3 (MIC19)	Thermo Fisher Scientific	Cat #: MA5-26597, RRID: AB_2724134
Rabbit Polyclonal anti-CPT2	Millipore	Cat #: ABS85, RRID: AB_11204869
Mouse Monoclonal anti-MRP-L12	Santa Cruz Biotechnology	Cat #: sc-100839, RRID: AB_2235442
Rabbit Polyclonal anti-MTCO2	Proteintech	Cat #: 55070-1-AP, RRID: AB_10859832
Rabbit Polyclonal anti-ATP6	Proteintech	Cat #: 55313-1-AP, RRID: AB_2881305
Mouse cocktail anti-OxPhos	Thermo Fisher Scientific	Cat #: 45–8099, RRID: AB_2533835
Chemicals, peptides and recombinant proteins		
Collagenase, Type 1	Worthington	LS004197
Dispase II	Sigma-Aldrich	04942078001
Dulbecco's Modified Eagle Medium	Promega	Z3141
Fetal bovine serum	HyClone	SH30080.03
Opti-MEM	Gibco	31985070
Penicillin-Streptomycin	Sigma-Aldrich	P4333
Phosphate-buffered saline	Gibco	21600-069
BODIPY	Thermo Fisher Scientific	Cat # C2102
DAPI	Invitrogen	D1306
CellROX	Thermo Fisher Scientific	Cat #: C10422
MitoTracker Red	Cell Signaling Technology	Cat #: C9082
MitoTracker Green	Thermo Fisher Scientific	Cat #: M7514
Fluo-4 AM	Thermo Fisher Scientific	Cat #: F14201
TMRE	Cayman chemical	Cat #: C21426
Lipofectamine 2000	Invitrogen	11668030
TRIzol Reagent	Sigma-Aldrich	T9424
Saturated Phenol	Fisher Scientific	Cat #: BP1751I-100
Chloroform	VWR Chemicals	BDH1109
Phenol/Chloroform/Isoamyl Alcohol	Fisher Scientific	Cat #: BP1752I-400
Methanol	Fisher Scientific	A412-20
NP-40	Thermo Fisher Scientific	85124
SDS (Sodium Dodecyl Sulfrate)	Fisher Scientific	02-004-080
Sodium Azide	Fisher Scientific	BP922I-500
PMSF	Calbiochem	7110-OP
Paraformaldehyde	Sigma-Aldrich	P6148
Critical commercial assays		
M-MLV reverse transcriptase	Invitrogen	28025021
Pierce BCA Protein Assay Reagent	Thermo Fisher Scientific	232225
Western Blotting Chemiluminescence Luminol Reagent	Santa Cruz Biotechnology	sc-2048

(*Continued on next page*)

Continued

REAGENT or RESOURCE	SOURCE	IDENTIFIER
Experimental models: Cell lines		
Mouse: Brown adipocyte cell line	Dr. Shingo Kajimura, Harvard Medical School	
Experimental models: Organisms/strains		
Mouse: Ucp1^{Cre}	The Jackson Laboratory	JAX Stock: #024670
Mouse: Letmd1$^{fl/fl}$	i-GONAD technique[69] courtesy of Dr. Pengpeng Bi, University of Georgia	
Mouse: Letmd1^{KO} (Global)	Snyder et al.[7]	
Oligonucleotides		
See Table S2	This paper	N/A
Recombinant DNA		
pCMV(CAT)T7-SB100	Addgene	RRID: Addgene_34879
pSBtet-Pur	Addgene	RRID: Addgene_60507
TurboID	A gift from Dr. Michael Rudnicki and David Datzkiw, University of Ottawa	
Deposited data		
ProteomeXchange Consortium	Data set identifier: PXD051679; PXD054844	
Software and algorithms		
Fiji-ImageJ	N/A	RRID: SCR_002285
PRISM 9.0	GraphPad Prism	RRID: SCR_002798
Proteome Discover	Version 2.3 (Thermo Fisher Scientific)	RRID: SCR_014477 Default software settings were used to perform proteomic analysis. No custom computer code was used.
Spectronaut	Version 17 Biognosys	Default software settings were used to perform proteomic analysis. No custom computer code was used.
Perseus	Version 2.0.7.0	RRID: SCR_015753 Default software settings were used to perform statistical analysis. No custom computer code was used.
R	Version 4.2.2 pheatmap and EnhancedVolcano packages were used	RRID: SCR_001905

EXPERIMENTAL MODEL AND STUDY PARTICIPANT DETAILS

Mice

Deletion of *Letmd1* in UCP1+ cells was generated by breeding *Ucp1*^{Cre} with a newly generated *Letmd1*$^{flox/flox}$ mouse strain. The *Letmd1*$^{flox/flox}$ mouse line was created using the *i*-GONAD technique[69] courtesy of Dr. Pengpeng Bi at the University of Georgia. Briefly, the CRISPR cocktail consisting of Cas9 protein, a pair of guide RNAs (GTTAATCGACCATGACGCCC and GCGAGGCCTACCACATATTC) and corresponding homology directed repair (HDR) templates were delivered to mouse zygotes through oviduct electroporation to allow for insertion of LoxP sites flanking exons 3–7 of *Letmd1*. Genotyping polymerase chain reaction (PCR) was conducted using genomic DNA isolated from the mouse ear. *Ucp1*^{Cre} genotyping PCR primers and program guidelines were provided by the supplier. Primer sequences for genotyping analysis of 5′ LoxP of *Letmd1* gene: TCTTCCGTCAGGGTTTGAGC, TGATAAACACGCCCCACGAA. WT band size is 307 bp; 5′ LoxP band size is 341 bp. Primer sequences for genotyping analysis of 3′ LoxP of *Letmd1* gene: CAGTGGCACAGAGCAGAGAA, ACACCTGT CGTCAGCAATGT. WT band size is 379 bp; 3′ LoxP band size is 413 bp. Successful germline transmissions of both LoxP sites were confirmed in the F1 generation progenies from breeding the F0 generation founder with WT mice. Correct LoxP insertions were detected by PCR and verified by Sanger sequencing using primers outside the HDR template regions (Figure S1). The genotype of conditional knockout mice is *Letmd1*^{UKO} (*Ucp1*^{Cre};*Letmd1*$^{flox/flox}$). The genotype of control (Ctrl) mice is *Letmd1*$^{flox/flox}$ and *Letmd1*$^{flox/+}$. All performed animal procedures were approved by institutional Animal Care and Use Committees at the University of Georgia (IACUC) and Purdue university (PACUC). Mice were housed in an animal facility with free access to water and standard rodent chow. For all animal experiments, at least three pairs of

two-month-old, gender-matched littermates were used, aside from the developmental data shown in Figure 1G. Prior to euthanasia, mice were anesthetized with 3% isoflurane, followed by cervical dislocation.

Stromal vascular fraction (SVF) isolation and protein import assay

Upon dissection, BAT was briefly minced and placed in digestion media (2.4 mg Dispase II, 3.13 mg Collagenase Type I, 2.5 mL DMEM/mouse), for approximately 30 min in a 37°C water bath, to allow for density separation. Samples were vigorously shaken every 10 min to monitor digestion completion. Digestion was terminated with addition of DMEM, and samples were filtered through a 40-μM filter to remove undigested tissue, followed by a 5-min centrifugation at 1,800 rpm to isolate SVF cells in the sediment. SVF cells were seeded in growth medium containing DMEM, 20% FBS and 1% penicillin/streptomycin (P/S) at 37°C with 5% CO_2. Fresh medium was added every two days. Once 50% confluency was reached, SVF cells were transfected with Cox8 (MTS)_GFP fusion protein, consisting of the mitochondrial targeting sequence (MTS) for IMM protein Cox8 ('N#1-MSVLTPLLLRSLTGSARRLMVPRAQ-#25C') fused to the N-terminus of GFP. After transfection for 48 hours, doxycycline was added at a concentration of 1:5000 (1mg/mL stock) for an additional 48 hours before immunofluorescence staining using a Leica DM6000B microscope.

Mature adipocyte isolation

Upon dissection, BAT was briefly minced and placed in digestion media (2.4 mg Dispase II, 3.13 mg Collagenase Type I, 2.5 mL DMEM/mouse), for approximately 30 min in a 37°C water bath, to allow for density separation. Samples were vigorously shaken every 10 min to monitor digestion completion. Digestion was terminated with addition of DMEM, and samples were filtered through a 70-μM filter to remove undigested tissue, followed by a 5-min centrifugation at 2,500 rpm. After centrifugation, approximately 4 mL of medium was collected from the top, cloudy layer, placed in a 15 mL Falcon tube and spun at 1,800 rpm for 5 min. Approximately 2 mL was then collected from the top, cloudy layer, placed into a 2 mL microcentrifuge tube and spun at 100 rpm for 5 min. After centrifugation, a P1000 and P20 pipette tip were stacked and inserted to the bottom of the microcentrifuge tube to aspirate all media except the top, cloudy layer. 1 mL of DMEM was added to resuspend the layer, followed by a 5-min spin at 100 rpm. The process of aspirating media, resuspending the top layer in DMEM and centrifugation was repeated twice, followed by aspiration of media from the bottom layer. Desired stains were added to the top layer of each sample, followed by a 30 min incubation at 37°C, a final wash and centrifugation. Cells from the top layer were briefly resuspended in DMEM and placed on slides for visualization using a Leica DM6000B microscope.

METHOD DETAILS

Hematoxylin-Eosin (H&E) staining

Adipose tissues, kidney and brain from Ctrl and *Letmd1*^{UKO} mice were fixed in 4% Paraformaldehyde (PFA) overnight at 4°C. Once dehydrated in a series of graded ethanol and cleared with xylene, the tissues were embedded into paraffin, blocked, and cut at 5 μm. For H&E staining, the sections were deparaffinized and rehydrated, and the nuclei were then stained with hematoxylin for 15 min. Sections were rinsed in running tap water, stained with eosin for 3 min, dehydrated, and mounted. Images were captured using a Leica DM6000B fluorescent microscope.

Protein extraction and western blot

Protein was extracted from brown adipose tissue with RIPA buffer (150 mM NaCl, 50 mM Tris-HCl (pH 8.0), 1% NP- 40, 0.5% sodium deoxycholate, 0.1% SDS) supplemented with proteinase inhibitor and phenylmethylsulphonyl fluoride (PMSF). Supernatant protein concentration was quantified using Pierce BCA Protein Assay Reagent. Proteins were separated by electrophoresis and transferred onto a polyvinylidene fluoride (PVDF) membrane. After transferring, membranes were blocked in 5% fat-free milk for 1 hr at room temperature, followed by overnight primary antibody incubation at 4°C. The following day, membranes were washed in 1X TBST (0.02% Tween-20) before a 1hr incubation in secondary antibody at room temperature. Additional washes in 1X TBST (0.02% Tween-20) were performed before membranes were visualized using a chemiluminescent luminol reagent.

RNA extraction and quantitative PCR (qPCR)

Total RNA was extracted from tissues using Trizol reagent according to the manufacturer's instructions. The purity and concentration of total RNA was measured by a spectrophotometer (nanodrop 2000, Thermo Fisher). 3 μg of total RNA from each sample was reverse transcribed using random primers and M-MLV reverse transcriptase (Invitrogen) in an Applied Biosystems Verity 96 Well Thermal Cycler. qPCR was conducted in a Roche Lightcycler 96 PCR system using SYBR Green Master Mix and gene-specific primers listed in Table S2. Primers used include *qUcp1*The $2^{-\Delta\Delta CT}$ method was used to analyze the relative changes in gene expression normalized against mouse 18S rRNA as an internal control.

Glucose and insulin tolerance tests

For glucose tolerance test, mice were intraperitoneally injected with 0.1 g/ml d-glucose (2g/kg bodyweight normal chow diet, 1g/kg high-fat diet) after fasting for 14 h overnight. Blood glucose measurements were taken at 0, 15, 30, 45, 60, 75, 90, 105, and 120 min post-injection. For insulin tolerance test, mice were fasted for 4 h and then intraperitoneally injected with human insulin (Santa Cruz Biotechnology) (0.75U/kg

bodyweight normal chow diet and high-fat diet). Blood glucose measurements were measured using a glucometer (Accu-Check Active, Roche) and were taken at 0, 30, 60, 90, and 120 min. Blood from the tail vein of each mouse was dropped onto a glucose test strip and measured with a glucometer. All measurements for both GTT and ITT were double blinded.

Cold and thermoneutral exposure experiments

Two-month-old mouse pairs underwent both acute and chronic cold exposure experiments in an environmental chamber (Memmert, HPP260) set at 6°C. Mice were monitored for changes in behavior, including excessive shivering, lethargic movements and lack in responsiveness to touch.

Acute cold exposure with fasting lasted for 6 h, after which mice were removed from the chamber. Chronic cold exposure lasted seven days, after which mice were euthanized for sample collection. One mouse was housed per cage during cold exposures and nesting paper was removed. Rectal temperature was collected at the stated time using a digital thermometer (ETI, MicroTherma2) and copper thermocouple probe (TypeT). For intrascapular BAT temperature recording, mice were first injected (10 μL/g) with ketamine (0.9 mg/mL). A sterile, 21 gauge needle was inserted into the left or right portion of BAT, and a copper thermocouple probe (TypeT) was placed inside the needle opening to reach the BAT. For each mouse, a temperature reading was taken for both the left and right portion of BAT. The two readings were averaged and recorded.

Transmission electron microscopy (TEM) imaging

Upon dissection, BAT samples were immediately fixed in 2.5% glutaraldehyde and 2% paraformaldehyde in a 0.1 M sodium Cacodylate buffer overnight at 4°C. After washing in the same buffer, tissues were fixed in 1% Osmium Tetroxide and 0.8% Ferricyanide buffered in dH2O for 2 h, and stained with 1% Uranyl Acetate in dH2O for 1 hr at RT. Tissue samples were then dehydrated through a graded series of ethanol and 100% Acetonitrile. Infiltration was performed by incubating the tissue samples in acetonitrile and resin at a ratio of 2:1, overnight. Samples were changed to acetonitrile and resin at a ratio of 1:2, and then changed to 100% resin for 2 h, before polymerization at 60°C over-night. Sections (90 nm) were prepared with uranyl acetate and lead citrate stain and imaged at 120 kV with Tecnai T12 transmission electron microscope attached with a Gatan imaging system.

DNA extraction and relative mitochondria copy number

BAT was digested in 500 μL of DNA extraction buffer (10 mM Tris-HCl, pH 8.0, 1% SDS, 50 mM EDTA, 50 μg Proteinase- K) overnight at 55°C. After digestion, genomic DNA was extracted using a phenol chloroform method. In brief, equal volume of phenol was added to the sample, following centrifugation at 12,000 rpm for 20 min at 4°C to generate different liquid phases. The top phase containing DNA was transferred to a new tube and the same volume of a phenol:chloroform:isoamyl solution (25:24:1 ratio) was added, followed by a 15-min spin with the same settings. The same volume of a chloroform:isoamyl solution (24:1 ratio) was added to the top layer and spun at 10,000 rpm for 15 min. DNA was precipitated from the top layer by the addition of 1/10 volume of 3 M NaAc, 2X volume of precooled 100% EtOH, and pelleted by centrifugation at 10,000 rpm for 10 min. The supernatant was aspirated and 30 μL dH2O was added to each remaining pellet. The concentration and quality of genomic DNA were measured by a spectrophotometer (Nanodrop 2000, Thermo Fisher) and subjected to further qPCR analysis. To quantify the amount of mtDNA, we used the following *mt-Nd2* primers: Forward: CCTATCACCCTTGCCATCAT; Reverse: GAGGCTGTTG CTTGTGTGAC. To quantify nuclear DNA, we used a primer set that detects the *Pecam* gene on chromosome 6: Forward: ATGGAAAGCCT GCCATCATG; Reverse: TCCTTGTTGTTCAGCATCAC.

TurboID proximity labeling

Construction of a fusion protein linking *Letmd1* and TurboID, was performed using Gibson assembly.[23] This fusion protein has TurboID linked to the C-terminus of *Letmd1* cDNA, and the amino acid sequence GGGGSGGG was inserted between *Letmd1* and TurboID as a linker. The fusion protein was cloned into the pSBtet-Pur plasmid (Addgene #60507), which harbors the Tet-on induced expression system, allowing us to subject a brown adipocyte cell line, generously gifted by Dr. Shingo Kajimura, to doxycycline-induced expression of the fusion protein. Cells were co-transfected with the pSBtet-Pur plasmid and a sleeping beauty transposon system (100x sleeping beauty transposase, pCMV(CAT) T7-SB100, Addgene #34879), which was used to generate a stable transfected cell line. Two control groups were applied to transfected cells: 1. Uninduced, biotin-treated cells and 2. Induced, biotin-free cells. Induced cells treated with biotin for five minutes served as our experimental group. Cells were then collected, followed by mitochondria isolation, protein extraction, and incubation with streptavidin magnetic beads to capture biotinylated proteins. In the second TurboID proximity labeling experiment, a separate fusion protein, consisting of the mitochondrial targeting sequence (MTS) for IMM protein Cox8 ('N#1-MSVLTPLLLRSLTGSARRLMVPRAQ-#25C') fused to the N-terminus of TurboID, served as a labeling control.

Isolation of BAT cytosolic and mitochondrial fractions

Isolation of cytosolic and mitochondrial fractions from BAT was performed as previously described.[70] Upon dissection, BAT was wash thoroughly in cold 1X PBS, resuspended in 500 μL of STM buffer and homogenized on ice for 1 min. After incubating on ice for 30 min, samples were spun at 800g for 15 min. The resulting nuclear pellet was discarded, and the supernatant was spun at 800g for 10 min, followed by centrifugation at 11,000g for 10 min. The resulting pellet was resuspended in 100 μL STM buffer and spun at the same setting to obtain the

mitochondrial pellet. The supernatant remaining from the initial spin at 11,000g was precipitated in cold 100% acetone for 1 hr at 20°C, then spun at 12,000g for 5 min to obtain the cytosolic pellet.

Isolation of mitochondrial protein aggregates

Isolation of soluble and insoluble protein was conducted as previously described.[71] Briefly, cytosolic and mitochondrial pellets were resuspended in Lysis Buffer (25 mM Tris-HCl, 300 mM NaCl, 5 mM EDTA, 1% phenylmethylsulfonyl fluoride (PMSF), 1% proteinase inhibitor) + 1% NP-40, incubated on ice for 10 min and spun at 20,000g for 30 min. The resulting supernatant contained soluble protein, and concentration was determined using BCA analysis. Pellets containing insoluble protein aggregates were resuspended in Lysis Buffer + 1% NP-40 and spun at 20,000g for 15 min. Resulting pellets were resuspended in Lysis Buffer for protein extraction and BCA analysis.

Sample preparation for mass spectrometry-based proteomic analyses

Mitochondria isolation from Ctrl and Letmd1^{UKO} brown fat

Isolated Ctrl and *Letmd1^{UKO}* mitochondrial pellets were resuspended in PTS lysis solution (12 mM sodium deoxycholate, 12 mM sodium lauroyl sarcosinate, 100 mM triethylammonium bicarbonate buffer (TEAB), 10 mM tris(2-carboxyethyl)phosphine (TCEP), 40 mM chloroacetamide (CAA)) for phase transfer surfactant (PTS)-aided enzymatic digestion. The samples were incubated at 95°C for 5 min with periodic shaking. Samples were then sonicated for 10 consecutive, 1-second rounds. The incubation and sonication of samples was repeated once more before centrifugation at 16,000g for 10 min. After BCA analysis of protein concentration, the samples were diluted five-fold with 50 mM TEAB and digested with trypsin (Thermo Scientific) at 1:50 (w/w) enzyme-to-protein ratio at 37°C with overnight shaking. The following day, samples were acidified with trifluoroacetic acid (TFA) to a final concentration of 1% (v/v). Ethyl acetate solution was then added at a 1:1 ratio to the samples, and the mixture was vortexed for 2 min and then centrifuged at 20,000g for 2 min to obtain aqueous and organic phases. The organic phase (top layer) was removed, and the aqueous phase was collected. This surfactant removal step was repeated one more time. The aqueous phase was dried down to <10% original volume in a vacuum centrifuge and desalted using in-house prepared C18 tips (Sorbtech). The peptide concentration was determined using the Pierce™ Quantitative Colorimetric Peptide Assay (Thermo Scientific) according to the manufacturer's instructions. 0.5 μg of the peptide from each sample was aliquoted and dried in a vacuum centrifuge for LC-MS/MS analysis.

TurboID proximity labeling

The magnetic beads with captured biotinylated proteins were resuspended in PTS lysis solution and incubated at 95°C for 10 min with shaking. After five-fold dilution with 50 mM TEAB, the samples were digested with trypsin at 37°C with overnight shaking. The following day, beads were removed using a magnetic separation rack, and the supernatant was acidified with TFA. The samples were then subjected to the surfactant removal step using ethyl acetate extraction, and the aqueous phase was dried down to <10% original volume in a vacuum centrifuge. After desalting and peptide concentration measurement, 0.5 μg of the peptide from each sample was aliquoted and dried for LC-MS/MS analysis.

Soluble and insoluble proteomes from cytosolic and mitochondrial fractions

TEAB, TCEP, and CAA were added into the soluble and insoluble protein samples to final concentrations of 100 mM, 10 mM and 40 mM, respectively. Proteins were further denatured, reduced and alkylated by incubating the samples at 95°C for 10 min with shaking. To perform single-pot, solid-phase-enhanced sample preparation (SP3), magnetic beads (Promega) were added to the samples. Acetonitrile was then added to the samples to a final concentration of 70% (v/v). After removing the supernatants, the beads were further washed with 95% acetonitrile twice and 70% ethanol twice. The resulting bead samples were reconstituted in 100 mM TEAB and digested with trypsin at 37°C with overnight shaking. Peptide-containing supernatants were collected and acidified with TFA. After the samples were desalted, peptide concentration was determined. 0.5 μg of the peptide from each sample was aliquoted and dried for LC-MS/MS analysis.

LC-MS/MS and raw data analyses

Mitochondria isolation from Ctrl and Letmd1^{UKO} brown fat

For the isolated Ctrl and *Letmd1^{UKO}* mitochondria samples, dried peptides were dissolved in 0.05% trifluoroacetic acid (TFA) with 2% (v/v) acetonitrile and injected into an Ultimate 3000 nano UHPLC system (Thermo Fisher Scientific). Peptides were captured on a 2 cm Acclaim PepMap trap column and separated on a heated 50 cm Acclaim PepMap column (Thermo Fisher Scientific) containing C18 resin. The mobile phase buffer included 0.1% formic acid (FA) in HPLC grade water (buffer A) with an eluting buffer containing 0.1% FA in 80% (v/v) acetonitrile (buffer B) run with a linear 70 min gradient of 6–30% buffer B at a flow rate of 300 nL/min. HPLC was coupled online with a QExactive HF-X mass spectrometer (Thermo Fisher Scientific). The mass spectrometer was operated in the data-dependent mode, in which a full-scan MS ranging from m/z 375 to 1,500 with a resolution of 60,000 was followed by MS/MS of the 15 most intense ions (30,000 resolution; normalized collision energy—28%; automatic gain control target [AGC]—2E4, maximum injection time—200 ms; isolation window −1.6 m/z; 60 s exclusion). The raw files were searched against the mouse database using Byonic and Sequest search engines in Proteome Discoverer 2.3 software (Thermo Fisher Scientific). MS1 precursor mass tolerance and MS2 tolerance were set at 10 and 20 ppm, respectively. A static modification was set as carbamidomethylation of cysteines (+57.0214 Da), and variable modifications were set as oxidation (+15.9949 Da) on methionine

residues, acetylation (+42.011 Da) at the N terminus of proteins. Search was performed with full trypsin/P digestion rule and allowed a maximum of two missed cleavages on the peptides. The false-discovery rates of proteins and peptides were set at 0.01. All data were quantified using the label-free quantitation node (Precursor Ions Quantifier) through the Proteome Discoverer. The intensities of peptides were extracted with 10 ppm as initial precursor mass tolerance, 2 as minimum number of isotope peaks, 0.2 min as maximum ΔRT of isotope pattern multiplets, 0.01 as PSM confidence FDR, ANOVA hypothesis test, 5 min as maximum RT shift, pairwise ratio-based calculation, 100 as maximum allowed fold change, and total peptide amount as normalization mode.

TurboID proximity labeling, soluble and insoluble proteomes from cytosolic and mitochondrial fractions

For the TurboID, cytosolic and mitochondrial samples, dried peptides were dissolved in 0.1% FA and loaded onto Evotips Pure (EvoSep) according to the manufacturer's instructions. Peptides were then analyzed by the Evosep One LC system (EvoSep) coupled with a timsTOF HT mass spectrometer (Bruker). The Whisper40 SPD method was used with the PepSep C18 column (15 cm x 75 μm, 1.9 μm; Bruker) at 50°C inside a Captive Spray source (Bruker) equipped with a ZDV Sprayer 20 μm emitter (Bruker). The mobile phases included 0.1% FA in LC–MS grade water as buffer A and 0.1% FA in acetonitrile as buffer B. The timsTOF HT was operated in dia-PASEF mode with variable window widths covering an m/z range from 300 to 1,200. The ion mobility (IM) range was set to 1.5 and 0.6 V cm^{-2}. The accumulation and ramp times were specified as 100 ms, and the dia-PASEF method with 12 scans has a cycle time of 1.38 s. The collision energy was set from 59 eV at 1.6 V cm^{-2} to 20 eV at 0.6 V cm^{-2}. The raw files were searched against the mouse database using a directDIA (library-free) method in Spectronaut™ v17 software (Biognosys). In Pulsar search engine, criteria included trypsin/P as specific digest type, 5 minimal peptide length, 52 maximum peptide length, carbamidomethyl at cysteine as fixed modification, acetyl protein N-term and oxidation at methionine as variable modifications, and 5 as maximum variable modifications were applied. The FDR at PSM, peptide, and protein group were set to 0.01. Retention time prediction with local regression calibration was used. The identification was determined with mutated decoy generation and dynamic size at 0.1 fractions of library size. The quantitation was performed at the MS2 level, and cross-run normalization was enabled. Qvalue and no imputing were used as data filtering. All mass spectrometry data have been deposited to the ProteomeXchange Consortium via the jPOST partner repository with the dataset identifier PXD051679; PXD054844.

Bioinformatics analysis

The identified proteins in all datasets were filtered by the MitoCarta3.0 database to only include mitochondrial proteins.[72] For TurboID data, the identified proteins in uninduced, biotin-treated samples were first used to filter out background biotinylation. The data were then analyzed in the Perseus software (version 2.0.7.0) using the intensities of mitochondrial proteins extracted from either Proteome Discoverer or Spectronaut search results. The data were log2-transformed, and quantifiable proteins were selected as identified by the three replicates in at least one condition. The imputation was performed by replacing the missing values of intensities to a normal distribution with a downshift of 1.8 SDs and a width of 0.3 SDs. The imputed data was further normalized by subtracting the median of all intensities in each individual sample from all the intensities. In the volcano plots, the significantly changed proteins were identified by the *p*-value and fold change. The vertical dotted line represents the fold change cutoff of 2.83 or 0.35 (log_2(difference)=±1.5) for isolated Ctrl and *Letmd1*^{UKO} mitochondrial samples and TurboID samples. The horizontal dotted line represents the two-sample t-test *p*-value cutoff of 0.01 (-log_{10}(*p*-value)=2). Visualizations of volcano plots were created using R (version 4.2.2). The GO Biological Process and Molecular Function analysis were performed using ShinyGO (VO.80).[73]

For insoluble and soluble whole cell mass spectrometry analysis, protein intensities were first normalized to the total intensity of each cytosolic and mitochondrial fraction biological replicate. Three biological replicates were used in total for each sample type (cytosolic soluble, cytosolic insoluble, mitochondrial soluble, mitochondrial insoluble). After total intensity normalization, the intensities of cytosolic and mitochondrial fractions were combined for each individual replicate. The data was then analyzed in Perseus software using the same workflow as described above, with the exception of the median normalization step. The significantly enriched proteins were identified using a *p*-value cutoff of < 0.01 and visualized in the heat maps created using R.

Blue native PAGE (BN-PAGE)

BN-PAGE was performed as previously described.[74] Briefly, mitochondrial pellets were resuspended in 40 μL Solubilization Buffer A (50 mM NaCl, 50 mM Imidazole/HCl, 2 mM 6-Aminohexanoic acid, 1 mM EDTA, pH 7.0) and 12 μL of 20% digitonin (w/v) followed by a 15-min incubation on ice. The samples were then centrifuged for 20 min at 20,000g, and 2 μL of supernatant was aliquoted for BCA analysis of protein concentration. 5 μL of 50% glycerol (w/v) and 6 μL of 5% Coomassie blue G-250 dye was added to the remainder of the supernatant, and the samples were stored at 80°C until the next day. The next day, samples were loaded on a 3%-12% Bis-Tris Gel (NativePAGE Novex). BN-PAGE was performed using Cathode Buffer B (50 mM Tricine, 7.5 mM Imidazole, 0.02% Coomassie blue G-250, pH 7.0) and Anode Buffer (25 mM Imidazole, pH 7.0) and run at 100V until sample had entered the gel, after which the voltage was increased to 500V. Once samples had run one-third of the total running distance, Cathode Buffer B was removed and replaced by Cathode Buffer B/10 (50 mM tricine, 7.5 mM Imidazole, 0.002% Coomassie blue G-250, pH 7.0) until the dye reached the bottom of the gel. Then the gel strip was used for 2D Tris-Glycine-SDS PAGE using a 10% separating gel. The gel strip was washed with 1% SDS for 15 min and then placed into the glass plates. Then the top of the glass plates was filled with 10% acrylamide native gel mixture. After running, the proteins were transferred onto a polyvinylidene difluoride (PVDF) membrane and the membrane was blocked with 5% skim milk prepared in 1X TBST (0.02% Tween-20) for 1 hr at RT and blocked with anti-LETMD1 and anti-OxPhos antibodies overnight, respectively.

QUANTIFICATION AND STATISTICAL ANALYSIS

All data are presented as mean ± standard error of the mean (SEM) for each experiment. Statistical analyses and graphing were performed using GraphPad Prism 8.0 (GraphPad Software). Immunofluorescence intensity measurements were quantified using ImageJ software. All analyses were made by two-tailed, Student's t- tests. Differences in data were considered significant at $*p < 0.05$, $**p < 0.01$, $***p < 0.001$, $****p < 0.0001$. a p value of <0.05 was defined as statistically significant, where as a p value greater than 0.05 was not considered significant.